

Article

Shear Force and Bending Moment Tuning Algorithm of Shuttle Tanker Model for Global Structural Analysis

Chaeog Lim ¹, Ik-seung Han ², Ju-Young Kang ³, Im-jun Ban ¹, Byungkeun Lee ¹, Jun Soo Park ⁴
and Sung-chul Shin ^{1,*}

- ¹ Department of Naval Architecture and Ocean Engineering, Pusan National University, Busan 46241, Republic of Korea; orc@pusan.ac.kr (C.L.); june3373@pusan.ac.kr (I.-j.B.); optilee@pusan.ac.kr (B.L.)
- ² Marine Renewable Energy Research Division, Korea Research Institute of Ships and Ocean Engineering, Daejeon 34103, Republic of Korea; ihan77@kriso.re.kr
- ³ Design Team, Bridge International Patent & Law Firm, Busan 48058, Republic of Korea; jyoung98@hanmail.net
- ⁴ Department of Naval Architecture and Ocean System Engineering, Kyungnam University, Changwon 51767, Republic of Korea; junsoopark@kyungnam.ac.kr
- * Correspondence: scshin@pusan.ac.kr

Abstract: Global ship analysis is conducted using a finite element model (FE model) for ship design and construction, which involves structural, motion, and vibration analyses. It is crucial to examine the structural safety of the hull and motion response. In the ship FE model used in global ship analysis, weight distribution is employed to adjust the light weight and center of gravity (COG), which are required to perform the analysis. Further, the FE model needs to satisfy the required longitudinal shear force (SF) and bending moment (BM) under the loading conditions of the ship. Moreover, the SF and BM in the ship Trim and Stability data are utilized to perform shear force tuning (SFT) and bending moment tuning (BMT) for the ship FE model. This ensures the ship model exhibits curves of the SF and BM that coincide with those of the ship. The SFT and BMT for the ship FE model are time-consuming and costly. Thus, to address these limitations, we propose an effective and accurate algorithm and program for SFT and BMT. Accordingly, we developed a C#-based algorithm to tune the weight, SF, BM, and COG of the ship FE model to the required target value. Finally, the accuracy of the newly developed algorithm was analyzed and compared by applying it to the shuttle tanker FE model under the ballast and full load conditions. Accuracy was within tolerance in both loading conditions. The average errors of SF and BM were smaller in the ballast condition than in the full load condition, and the errors were smaller at the bow than at the stern.

Keywords: longitudinal strength; ship FE model; shear force; bending moment; global ship analysis; algorithm



Citation: Lim, C.; Han, I.-s.; Kang, J.-Y.; Ban, I.-j.; Lee, B.; Park, J.S.; Shin, S.-c. Shear Force and Bending Moment Tuning Algorithm of Shuttle Tanker Model for Global Structural Analysis. *J. Mar. Sci. Eng.* **2023**, *11*, 1900. <https://doi.org/10.3390/jmse11101900>

Academic Editors: Bin Liu, Kun Liu and Chenfeng Li

Received: 13 August 2023

Revised: 22 September 2023

Accepted: 27 September 2023

Published: 29 September 2023



Copyright: © 2023 by the authors. Licensee MDPI, Basel, Switzerland. This article is an open access article distributed under the terms and conditions of the Creative Commons Attribution (CC BY) license (<https://creativecommons.org/licenses/by/4.0/>).

1. Introduction

With the increase in ship size and structural complexity, global ship analysis is conducted for shipbuilding upon the request of classification agencies and ship owners to evaluate structural safety and motion performance (Cho et al., 2008; Valtonen et al., 2020) [1–3]. High precision is required in global ship analysis to satisfy the needs of ship owners and achieve classification approval. Ship owners require global ship analysis results that can apply more specific and diverse loading conditions than before. Because the analysis results are used for classification approval and represent the competitiveness of the shipyard's analysis technology, global ship analysis has gained increasing importance for use in shipyards. The analysis is conducted using a finite element (FE)-based global ship model to consider the complexity of the analysis and various loading conditions (Kim et al., 2005; Park et al., 2007) [4,5]. A global ship FE model (referred to below as ship

FE model) implies an FE model of full size, and it consists of the ship structural members and main cargo tank. As the model excludes small secondary tanks, liquids, the outfit, and electric systems, its weight is different from that of the ship. Moreover, the ship FE model must have the same light weight and center of gravity (COG) as the actual ship to perform an accurate analysis, and the respective required target values are ensured through weight distribution (WD) (Lim et al., 2022) [6]. The target COG and weight are the value of the actual ship, and these values must be consistent with Trim and Stability (TnS) data of the ship. However, when the cargo state with the loading conditions for analysis is applied to the ship FE model that completed the WD, the longitudinal shear force (SF) curve and bending moment (BM) curve of the model do not match with those of the ship. For accurate analysis, the ship FE model must satisfy the longitudinal SF and BM curves of the ship under the loading conditions.

Owing to alternating hogging and sagging during the voyage, the BM of the ship is closely related to its structural safety. Thus, the SF and BM are significant factors in determining the structural safety of the ship (Kim et al., 2018; Liu and Guedes Soares, 2020; Wang et al., 2019) [7–9]. However, as the distribution of the SF and BM of the ship also affects the structural analysis results, a reliable method of tuning the SF and BM is needed. Therefore, shear force tuning (SFT) and bending moment tuning (BMT) are required for the ship FE model to tune the longitudinal SF and BM curves of the model to those of the ship TnS data. Here, the model COG and weight after SFT and BMT must satisfy the target values required for analysis, which are identical to those of the model that completed the WD.

Several studies on SF and BM have been conducted. Pesterev et al. (2001) [10] proposed a new method for calculating the BM and SF of proportionally damped beams owing to the movement of concentrated loads. This method was explained through its application to the moving oscillator problem. Wang et al. (2019) [9] designed a 10,000 TEU (Twenty-Foot Equivalent Unit) similar-scale model of a container ship and performed a numerical analysis on the structural strength and similar-scale models under the conditions of combined torsion and bending, pure torsion, and pure hogging bending. Based on the results and similarity theory, a similarity in ultimate strength between container ships and similar-scale models was proposed. Yun et al. (2020) [11] conducted a study to improve the existing analytical model used to forecast the nonlinear bending behavior of flexible risers. In contrast to previous analytical models, in the present study, a series of equilibrium equations were derived considering the radial and shear deformations of multiple layers. Further, to verify the proposed model, bending analysis was performed on a 2.5 in flexible riser, and the results were compared with the FE results. Kim et al. (2020) [12] proposed a multi-hysteresis modeling method to analyze the BM behavior of the riser extended to the global area. The proposed method used a realistic and accurate bending hysteresis curve considering shear deformation and axisymmetric load. Waskito et al. (2020) [13] measured the wave load on the surface of a ship model using a fiber Bragg grating pressure sensor attached to the ship. Comparisons and an analysis of the measured values and computational fluid dynamics results revealed them as being consistent with the nonlinear vertical BM. Kövesdi et al. (2016) [14] studied the effect of additional normal stress on the bending stress of trapezoidally corrugated webs. In particular, a study was performed on the determination of the transverse BM and its effect on the load transfer of trapezoidally corrugated webs. In addition, the structural behavior of a trapezoidally corrugated web girder under BM and SF was studied. Recuperero et al. (2005) [15] conducted a generalization study of prestressed and reinforced concrete models subjected to the interaction of SF, BM, and axial load. Biondi et al. (2004) [16] proposed two methods to capture discontinuities due to moving mass in the BM and SF laws along a continuous structure with varying accuracy. Kim et al. (2018) [7] calculated the secondary BM induced by sea waves using the secondary strip theory. It was found that the secondary BM changed significantly according to the change in the ship side angle. Liu and Guedes Soares (2020) [8] reported that the hull girder under the condition of the cyclic BM exhibited weaker ultimate strength

than the monotonically increasing BM. Further, the collapse modes of a hull girder under monotonic and cyclic loading were compared, revealing the cyclic ultimate load of the hull structure as being approximately 10% lower than the existing ultimate strength. Rahman and Chowdhury (1996) [17] developed the calculating method of the ultimate value of the longitudinal BM on the cross-section in the girder of the ship or box. The calculating method was developed using a FORTRAN program and tested on several box girder models and actual ships. Xu and Haddara (2001) [18] developed an artificial neural network (ANN) model to predict the vertical BM of the ship due to waves. The ANN learned the heave and pitch motions to estimate the vertical BM. Xu et al. (2019) [19] experimented on the ultimate strength of an inland catamaran under the condition of vertical BM. Further, an FE analysis of a scale model indicated that the ultimate BM obtained through analysis coincided with the experiment results. Mansour and d'Oliveira (1975) [20] developed a computerized procedure to predict the hull vertical BM owing to slamming. The developed equation was validated through its application to a mariner ship. Moreira and Soares (2020) [21] proposed a time-domain technique based on the ANN to estimate the regular wave-induced vertical BM and SF. The ANN was used to model the time-domain relationship between BM, SF, and ship motion. Lee et al. (2010) [22] suggested a three-dimensional source distribution method to estimate the motion and vertical BM of a ship advancing in a regular wave. In addition, the validity of the method was confirmed through comparisons of results with experimental values. Kwon (1996) [23] studied the effect of the hull WD on still-water bending and wave-induced BM. Kim and Paik (2003) [24] calculated and analyzed the wave-induced BM due to long- and short-term responses subjected to various sailing conditions and sea states for a very large crude oil carrier and capsized bulk carrier. Thus, most studies have emphasized the development of a calculation method for the SF and BM of a ship, numerical calculation of the SF and BM responses for the structure using FE analysis, and measurement of the SF and BM through experiments. Therefore, owing to the scarcity of studies related to practical methods for the SFT and BMT of a ship FE model, further research and development are necessary.

In shipyards, NASTRAN software has been primarily used for global ship analysis (MSC, 2018) [25]. Although Det Norske Veritas (DNV) classification increases due to the demands of ship owners, requests for structural research in shipyards, and classification approval, global ship analysis must be conducted using the DNV's Sesam tool instead of NASTRAN in certain cases. In the case of global ship analysis using NASTRAN, general-purpose software based on NASTRAN is available for SFT and BMT. In contrast, for global ship analysis using DNV Sesam, general-purpose software has not been developed; thus, several calculation sheets arbitrarily created in the preliminary design stage are used in each work process and project for SFT and BMT. This increases the time consumed and cost because the designer performs tuning through trial and error using calculation sheets. In addition, as calculation sheets are not created using a systematic method for SFT and BMT, human errors and bottlenecks can occur in DNV Sesam analysis using calculation sheets. To address this limitation, an effective algorithm and software that can quickly and accurately perform SFT and BMT must be developed. Therefore, in this study, an algorithm and software to tune the SF and BM of a ship FE model were developed for global ship analysis using DNV Sesam. The newly developed algorithm and software are used such that the target SF and BM, as well as the target weight and COG, are satisfied. C# language was used to build the program, and a full-scale ship FE model was used to validate the performance and accuracy of the algorithm.

2. Research Method

2.1. Algorithm Overview

The five-step algorithm for SFT and BMT is shown in Figure 1. The weight and COG were tuned to satisfy the required target values during SFT and BMT. In the first step, the data of a ship FE model and TnS information of the ship were saved. The TnS data comprise the actual ship information (weight, trim, and stability) and are calculated using only the

weight distribution information. Next, the ship FE model was apportioned according to the required locations of the SF and BM checks. Thereafter, the weight of the ship FE model was calculated, while the SF and BM were calculated at each division position (DP). Finally, the SF and BM of the ship FE model were changed and tuned, and the ship FE model was saved. The dimensions of all elements and the COG for the ship model are represented using the coordinate system in Figure 2.

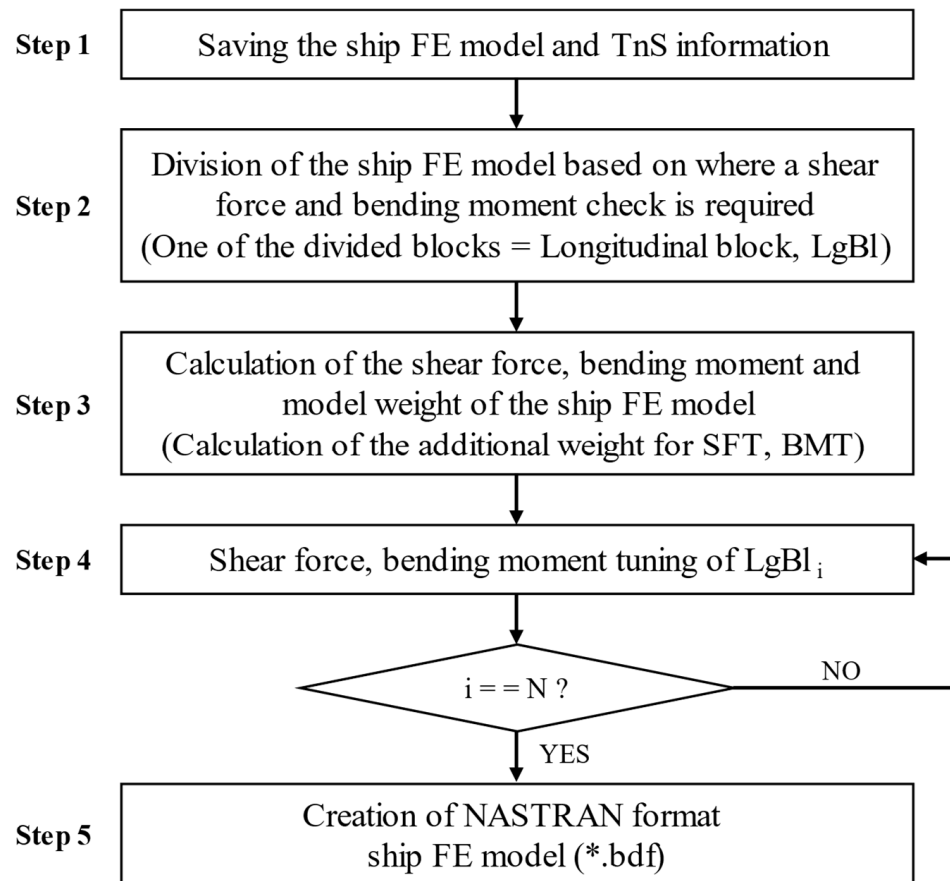


Figure 1. SFT and BMT algorithm.

Step 1: First, the TnS data and ship FE model were saved. The ship FE model comprises the coordinates, material properties, geometry, and dimensions of the elements. The weight of each structural member and the SF and BM of the ship FE model were calculated using these data and information in each step of the algorithm. The MSC NASTRAN 2018 Quick Reference Guide was used for calculating and handling the element data of the ship FE model (MSC, 2018). The TnS information contains the longitudinal WD information for each system, tank, liquid, and cargo of the ship and the information on longitudinal SF and BM. Step 2: Next, the ship FE model was divided in the longitudinal direction. The DPs were selected as the locations to check the SF and BM. The data on each divided model were then saved. An SF and BM check was required at each DP. Based on these positions, the ship FE model was split into N blocks. Each divided block is called a longitudinal block (LgBl), with a different length and size depending on the DP. Step 3: Using the data stored in each LgBl, the weight and COG of each LgBl and the ship FE model with the completed WD were calculated. The ship FE model weight was equal to the sum of the structural elements' weight and the additional weight ($AddWt$) added to the model because of the WD. Further, for model weight calculation, after calculating the element weight of each structural member, the weight was equally distributed to the grid of each element model that represented the coordinate data. The method of calculating the weight of the grid for a rectangular-shaped shell and a T cross-section beam is shown in Figure 3 and

Equations (1)–(1.b). The shell weight M_{shell} was divided into 4, and M_{shell} was allocated to *Grid1*, *Grid2*, *Grid3*, and *Grid4* of the shell element as $\frac{M_{shell}}{4}$ (Equation (1)). Similarly, the weight of a T cross-section beam is M_{beam} , and it consists of two grids. A weight of $\frac{M_{beam}}{2}$ was assigned to *Grid4* and *Grid5* of the beam (Equation (1.a)). *Grid4*, which is included in both the beam and shell, has an $\frac{M_{beam}}{2} + \frac{M_{shell}}{4}$ weight, as it takes the beam and shell. Further, the weight of $\frac{M_{beam}}{2}$ is distributed to *Grid5*, and the weight of $\frac{M_{shell}}{4}$ is distributed to *Grid1*, *Grid2*, and *Grid3*. Thus, the final weight was $\frac{M_{shell}}{4} + AddWt_{g1}$ for *Grid1*, $\frac{M_{shell}}{4} + AddWt_{g2}$ for *Grid2*, $\frac{M_{shell}}{4} + AddWt_{g3}$ for *Grid3*, $\frac{M_{beam}}{2} + \frac{M_{shell}}{4} + AddWt_{g4}$ for *Grid4*, and $\frac{M_{beam}}{2} + \frac{M_{shell}}{4} + AddWt_{g5}$ for *Grid5* (Equation (1.b)). Following the WD to all grids, the weight and COG of each LgBl model and the ship FE model weight and COG were calculated using the grid weight and coordinates of the model. In addition, the weight of the ship FE model was equal to the sum of the weights of all LgBl.

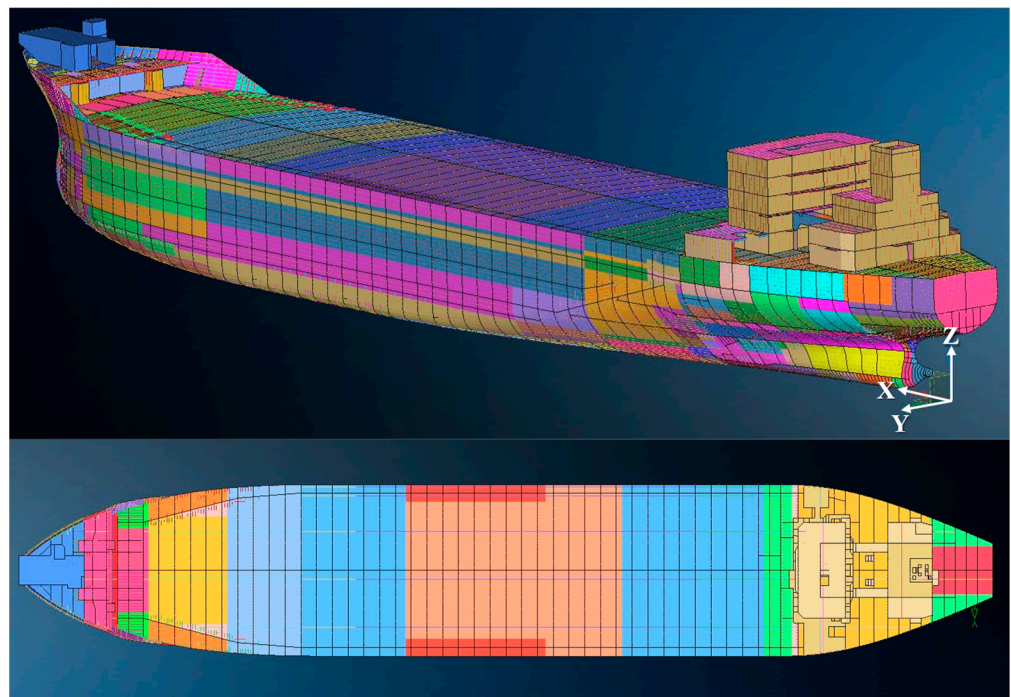


Figure 2. Coordinate system for all dimensions of the ship FE model.

$$m_{g1 \text{ of shell}}, m_{g2 \text{ of shell}}, m_{g3 \text{ of shell}}, m_{g4 \text{ of shell}} = \frac{M_{shell}}{4} \tag{1}$$

$$m_{g4 \text{ of beam}}, m_{g5 \text{ of beam}} = \frac{M_{beam}}{2} \tag{1.a}$$

$$m_{g1} = \frac{M_{shell}}{4} + AddWt_{g1}, m_{g2} = \frac{M_{shell}}{4} + AddWt_{g2}, m_{g3} = \frac{M_{shell}}{4} + AddWt_{g3} \tag{1.b}$$

$$m_{g4} = \frac{M_{beam}}{2} + \frac{M_{shell}}{4} + AddWt_{g4}, m_{g5} = \frac{M_{beam}}{2} + AddWt_{g5}$$

where

$$M_{shell} = \text{Shell weight}$$

$$M_{beam} = T - \text{beam weight}$$

$$m_{gj} = m_{gj \text{ of shell}} + m_{gj \text{ of beam}} + AddWt_{gj} : \text{Grid}_j \text{ weight}$$

$$AddWt_{gj} = \text{Additional weight of Grid}_j \text{ by WD}$$

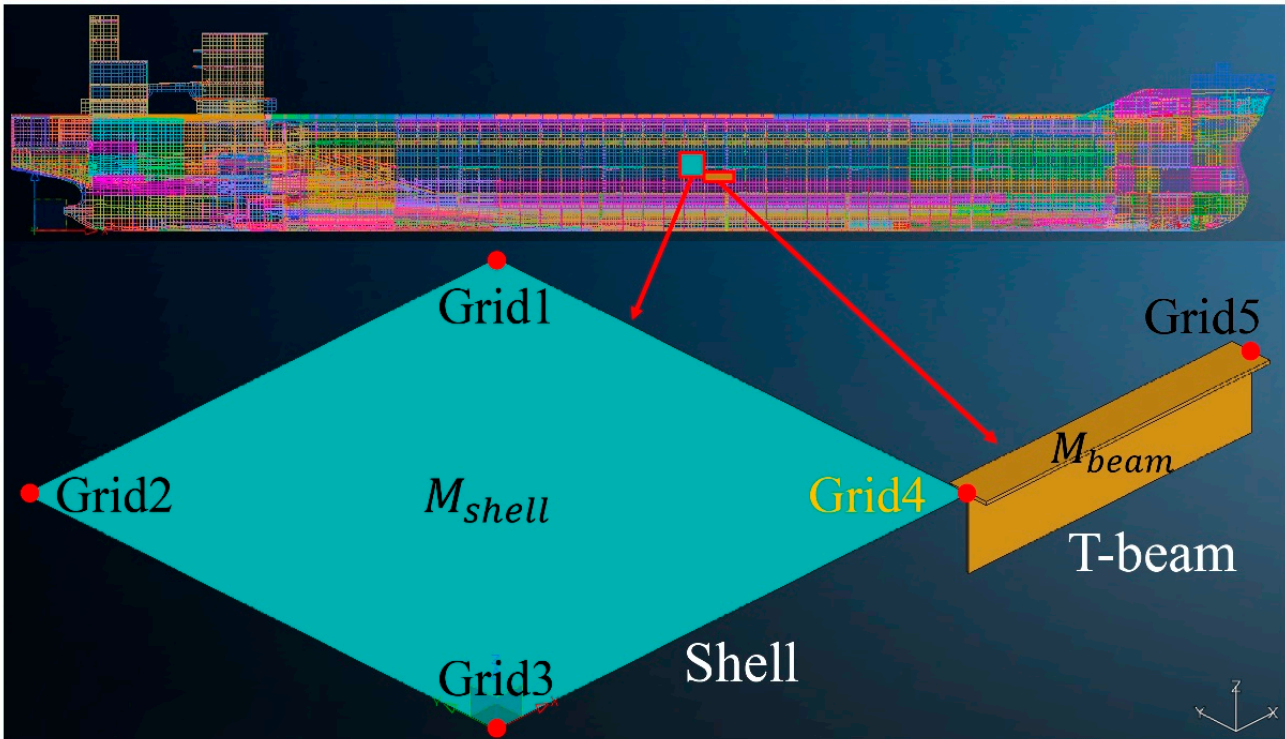


Figure 3. Calculation of grid weight of shell and T-beam elements with Equation (1).

The values of the SF and BM among the analysis results of the ship FE model with the WD completed were saved. Consequently, based on these values and the longitudinal SF and BM values of the ship obtained from the TnS data, the SFT and BMT values at each DP of the ship FE model were calculated. Here, the ship’s weights, SF, BM, and COG in the TnS data are target values of the ship FE model. The ship FE model satisfies the target value through SFT and BMT. Subsequently, considering these values and the grid weight information calculated above, the α additional weight (αWt) to be added or subtracted from each LgBl of the ship FE model for SFT and BMT was calculated. Steps 4 and 5: SFT and BMT were performed by distributing αWt to each LgBl in the direction from stern to bow. The SF and BM of the ship FE model that has completed tuning coincided with the SF and BM in TnS; that is, the SF and BM of the ship were the target SF and BM to be satisfied by the ship FE model. Finally, the algorithm was iterated until SFT and BMT were performed for all LgBl through the distribution of αWt . After tuning, the αWt information was saved as CONM2 cards, that is, the point mass of the grids, and consequently, a NASTRAN file format ship FE model containing the weight information was created (Lim et al., 2022) [6].

2.2. Detailed Process of the SFT and BMT

In Steps 3, 4, and 5 of Figure 1, the detailed process of SFT and BMT for the ship FE model that has completed the WD is as follows. Instead of performing SFT and BMT simultaneously, BMT was performed only when required after SFT. This is because a ship FE model that has completed the WD and SFT often satisfies the target values of the weight, COG, and SF at each DP, and thus has also satisfied the value of the BM under these conditions. However, BMT is required when the BM deviates from the target tolerance because of a slight difference in structural geometry between the model and ship, precision of the model data, or accuracy of the SFT values. Figure 4 shows the detailed process of SFT and BMT. If the target values of the SF and BM are obtained after SFT, tuning is completed.

Otherwise, BMT is performed, and tuning is completed if the target value is obtained after BMT. In the ship FE model coordinate system, “Xcog,” “Ycog,” and “Zcog” are the X—(longitudinal), Y—(transverse), and Z—(height) components of the COG location.

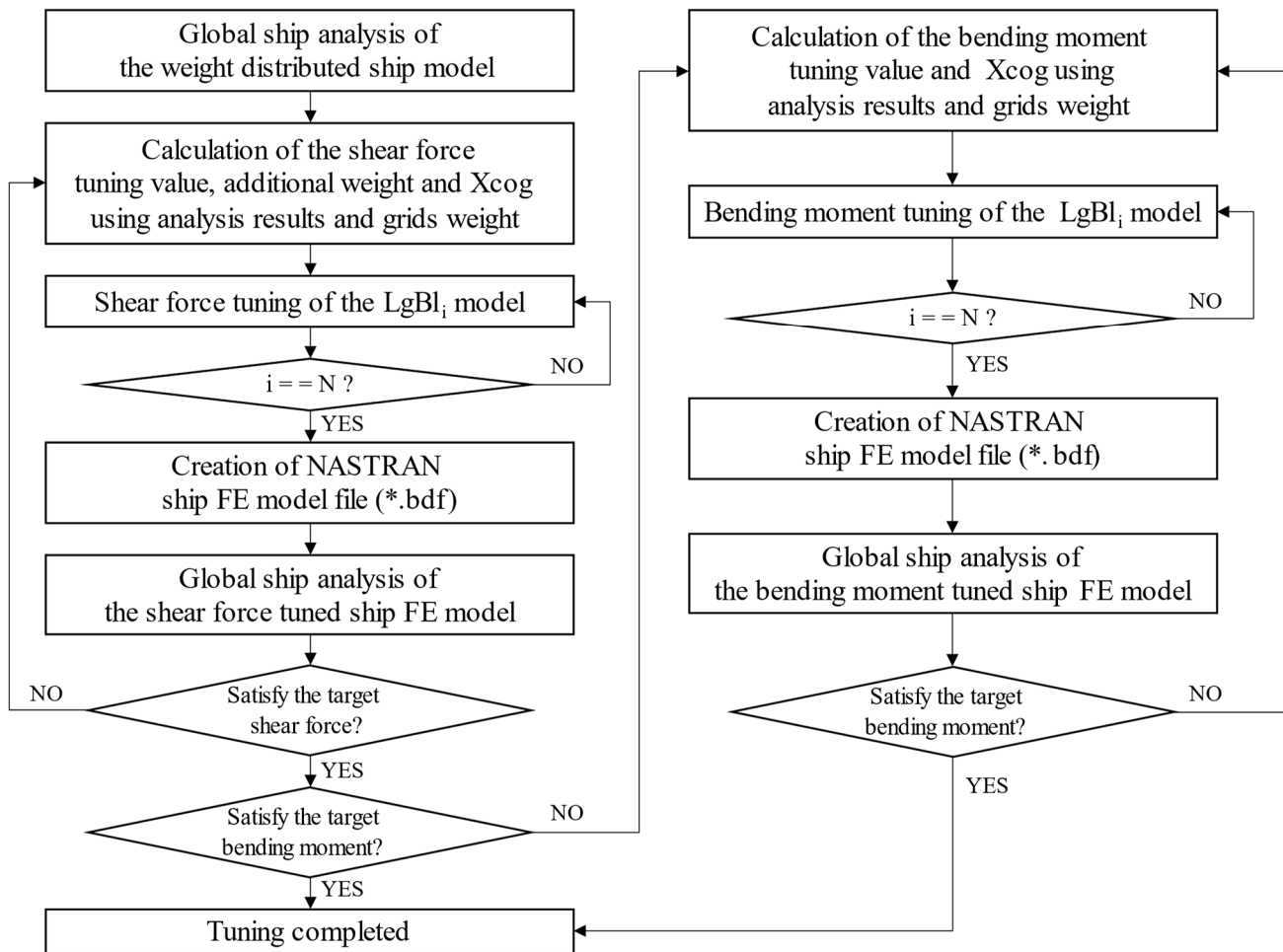


Figure 4. Detailed process for SFT and BMT in Steps 3, 4, and 5 of Figure 1. “Xcog” is the X-component of the ship FE model COG location.

2.2.1. Detailed Process of SFT

First, only SFT was performed for the ship FE model. Before the SF and BM were tuned for the ship FE model that completed the WD, they were significantly different from the target values. Thus, the SFT values at each DP of the ship FE model were calculated using the SF values of the ship FE model with WD analysis results, the longitudinal SF curve values of the TnS data, and the grid weight information. This is required to tune the SF of the current ship FE model to that of the actual ship. Based on the calculated value, αWt was added or subtracted from each LgBl of the ship FE model for SFT. Figure 5 and Equations (2)–(2.e) show the SFT value and the αWt calculation method when the number of DPs is three for the ship FE model, and the SF is calculated in the direction from the stern to the bow. Regarding LgBl₁ and the DP of p_1 , the SF increases by ΔSF_1 , and as a result, it changes from SF_1 to the target value SF'_1 (Equation (2)). Further, the weight of LgBl₁ changes from m_1 to m'_1 (Equation (2.a)). Moreover, when the SFs of LgBl₂ and p_2 and that of LgBl₃ and p_3 are adjusted in a similar manner, the SF of the ship FE model coincides with the TnS SF, which is the target value, and the total weight becomes equal to the target value, that is, the weight after WD Equations (2.b)–(2.e).

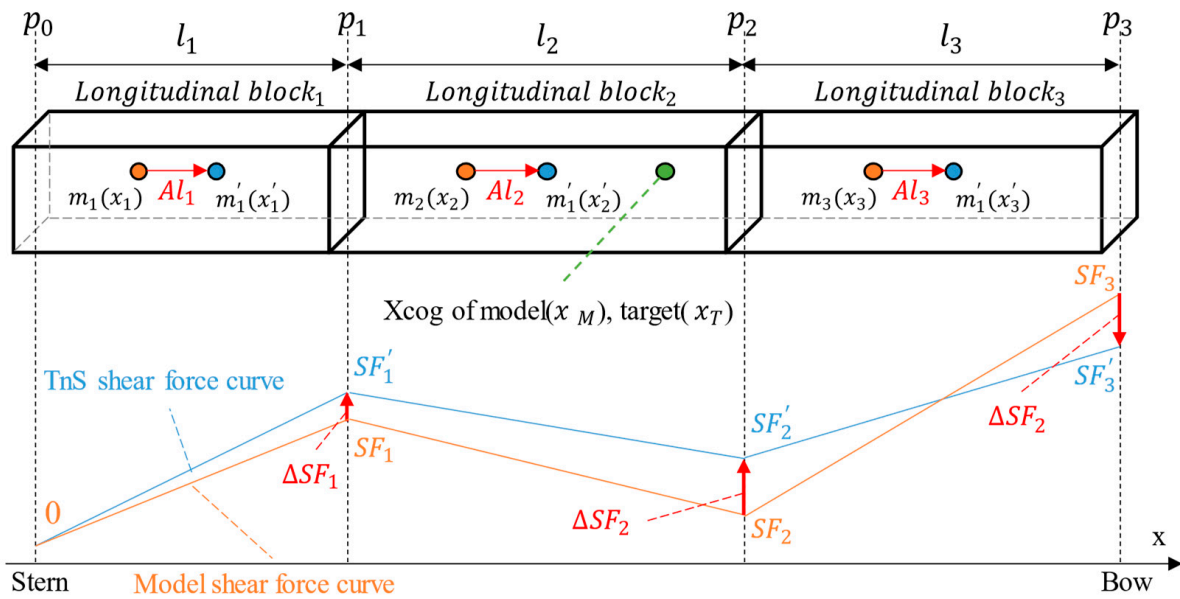


Figure 5. Calculation of the SFT value (ΔSF_i) using the TnS and model SF curve by global ship analysis. Calculation of the $LgBl_i$ target Xcog (x'_i) using a ratio A , to correspond to the ship FE model Xcog (x_M) to the target Xcog (x_T) through the SFT.

Prior to SFT, the ship FE model satisfies the target weight and COG because the WD has been completed. However, during SFT, the ship FE model COG is affected by the change in the COG of each LgBl. Therefore, when the SF is tuned by distributing the previously calculated αWt to each LgBl, the target COG that must be satisfied by each LgBl is calculated to tune the ship FE model COG to the target COG. When the target SF, weight, and Xcog are satisfied through SFT for all LgBl, those values associated with the completed SFT of the ship FE model will also satisfy the target values. Subsequently, the Ycog and Zcog of each LgBl were also tuned to the Ycog and Zcog of the ship FE model. The calculating method for the target Xcog of all LgBl when the ship FE model is separated into three LgBl parts is detailed in Figure 5 and Equations (3)–(3.c). The direction of the positive x-axis is the bow direction in Figure 5. Equation (3.c) shows the calculation method of A , which means the coefficient of Xcog moving the length of the LgBl. Further, regarding $LgBl_1$, the Xcog prior to SFT was x_1 with a weight of m_1 and a length of l_1 . After SFT, the Xcog moved by Al_1 from x_1 to x'_1 and the weight was m'_1 . Thus, when the Xcog of all LgBl is changed by Al_i in the same method, the Xcog of the ship FE model, x_M , coincides with the target value of x_T . Moreover, the total weight of the ship FE model, M , is maintained and coincides with the target value of M' . In addition, as the Ycog and Zcog of each LgBl are identical to the target values, the transverse (Ycog) and height (Zcog) components of the ship FE model COG location also coincide with the target values.

$$\Delta SF_1 = SF'_1 - SF_1 \tag{2}$$

$$m'_1 = m_1 + \Delta SF_1 \tag{2.a}$$

$$\Delta SF_2 = SF'_2 - SF_2 \tag{2.b}$$

$$m'_2 = m_2 + \Delta SF_2 - \Delta SF_1 \tag{2.c}$$

$$\Delta SF_3 = SF'_3 - SF_3 \tag{2.d}$$

$$m'_3 = m_3 + \Delta SF_3 - \Delta SF_2 \tag{2.e}$$

$$x_M = \frac{m_1x_1 + m_2x_2 + m_3x_3}{M} = x_T \tag{3}$$

$$x_T = \frac{m'_1x'_1 + m'_2x'_2 + m'_3x'_3}{M'} = x_M \tag{3.a}$$

$$\begin{aligned} x_T M' &= m'_1(x_1 + Al_1) + m'_2(x_2 + Al_2) + m'_3(x_3 + Al_3) \\ &= A(m'_1l_1 + m'_2l_2 + m'_3l_3) + m'_1x_1 + m'_2x_2 + m'_3x_3 \end{aligned} \tag{3.b}$$

$$A = \frac{x_T M' - (m'_1x_1 + m'_2x_2 + m'_3x_3)}{m'_1l_1 + m'_2l_2 + m'_3l_3} \tag{3.c}$$

where

m_i = Weight of LgBl_i model before SFT

m'_i = $m_i + \alpha Wt_i$ (Weight of LgBl_i model after SFT)

αWt_i = α additional weight of LgBl_i for SFT (αWt)

p_i = i DP

x_i = Xcog of LgBl_i model before SFT

x'_i = $x_i + Al_i$ (Xcog of LgBl_i model after SFT)

SF_i = Model shear force at p_i

SF'_i = TnS shear force at p_i

ΔSF_i = STF value

x_M = Xcog of the global ship model

x_T = Target Xcog of the global ship model ($x_M = x_T$, in SFT)

$M = m_1 + m_2 + m_3$ (Weight of the global ship model before SFT)

$M' = m'_1 + m'_2 + m'_3$

(Weight of the global ship model after SFT) ($M = M'$, in SFT)

l_i = Length of LgBl_i model

A = Length of a ratio used to set the Xcog of LgBl model after SFT

Figures 6 and 7 show the detailed process of weight addition to each $LgBl_i$ for SFT, and the description is as follows. Figure 7a–c show one $LgBl_i$, where the current Xcog of the $LgBl$ is x_i , and the target Xcog is x'_i . The $LgBl$ was divided into two based on x_i , as shown in Figure 7a, and the right side of the $LgBl$ is referred to as partial block 1 (PB1), while the left side is partial block 2 (PB2). The weight and Xcog of PB1 are m_{x1} and x_{p1} , and those of PB2 are m_{x2} and x_{p2} , respectively. The weight added to $LgBl_i$ for SFT was αWt_i , calculated using Equations (2)–(3.c). At this time, the weights added to PB1 and PB2 are Δm_{x1} and Δm_{x2} , respectively. As shown in Figure 7, for x_i to coincide with x'_i , x_i must be moved to the right by Al_i . Furthermore, Δm_{x1} and Δm_{x2} were calculated using Equation (4), and only Δm_{x2} was added to x_{p2} of PB2. In this case, Δm_{x1} was not added to PB1 because its value is zero. By contrast, if x'_i is on the left side of x_i , only Δm_{x1} is added to x_{p1} of PB1 because x_i must be moved to the left by Al_i . Similarly, Δm_{x2} is not added to PB2 because its value is zero. To satisfy the Xcog, Ycog, and Zcog target values, only 10% of Δm_{x1} and Δm_{x2} were added to the partial block. Further, 10% weight was added to each grid included in the partial block, as calculated using Equations (5)–(5.a). The weight added to the grid was calculated based on the ratio of the current grid weight to the current $LgBl$ weight. Thus, the above process is a method to achieve the Xcog target value during SFT. The SFT, Ycog, and Zcog adjustments are similar to that of the above Xcog method and are shown in Figure 7b,c, respectively. As evident, when adjusting the Ycog, the $LgBl$ is divided into left and right partial blocks based on the current Ycog (Figure 7b), whereas, when adjusting the Zcog, the $LgBl$ is divided into top and bottom blocks based on the current Zcog (Figure 7c). Furthermore, when SFT and adjustments are conducted in the order Xcog \rightarrow Zcog \rightarrow Ycog (1 iteration), and if COG (x_i, y_i, z_i) does not meet the target value (x'_i, y'_i, z'_i), the process is repeated.

$$\Delta m_{x1} = 0, \Delta m_{x2} = -\frac{(m_{x1} + \Delta m_{x1})(l_{x1} + Al_i) + m_{x2}(l_{x2} + Al_i)}{(l_{x2} + Al_i)} \tag{4}$$

where

$$l_{x1} = x_i - x_{p1}$$

$$l_{x2} = x_i - x_{p2}$$

$$Al_i = x'_i - x_i$$

$$x_i = \text{Current Xcog of } LgBl_i \text{ model}$$

$$x'_i = \text{Target Xcog of } LgBl_i \text{ model for SFT}$$

$$\Delta m_{x1} = \alpha \text{ additional weight of PB1 (Green area) for SFT}$$

$$\Delta m_{x2} = \alpha \text{ additional weight of PB2 (Blue area) for SFT}$$

$$m_{x1} = \text{Current weight of PB1}$$

$$m_{x2} = \text{Current weight of PB2}$$

$$\begin{aligned} \alpha Wt_{gjk} &= \frac{\text{Current weight of Grid}_j}{\text{Current weight of } LgBl_i} \times 0.1 \Delta m_{x2} \text{ (When : } \Delta m_{x1} = 0) \\ &= \frac{\text{Current weight of Grid}_j}{\text{Current weight of } LgBl_i} \times 0.1 \Delta m_{x1} \text{ (When : } \Delta m_{x2} = 0) \end{aligned} \tag{5}$$

$$\alpha Wt_{gj,k} = \alpha Wt_{gix,k} + \alpha Wt_{gij,k} + \alpha Wt_{giz,k} \tag{5.a}$$

where

$$\alpha Wt_{gj,k} = k^{th} \alpha \text{ additional weight of Grid}_j \text{ for SFT}$$

$$\alpha Wt_{gix,k} = k^{th} \alpha \text{ additional weight of Grid}_j \text{ for SFT, Xcog}$$

$$\alpha Wt_{gij,k} = k^{th} \alpha \text{ additional weight of Grid}_j \text{ for SFT, Ycog}$$

$$\alpha Wt_{giz,k} = k^{th} \alpha \text{ additional weight of Grid}_j \text{ for SFT, Zcog}$$

$k = \text{Iteration number}$

$$\Delta m_{x2} = \alpha \text{ additional weight of PB2 for SFT, Xcog}$$

$$\Delta m_{x1} = \alpha \text{ additional weight of PB1 for SFT, Xcog}$$

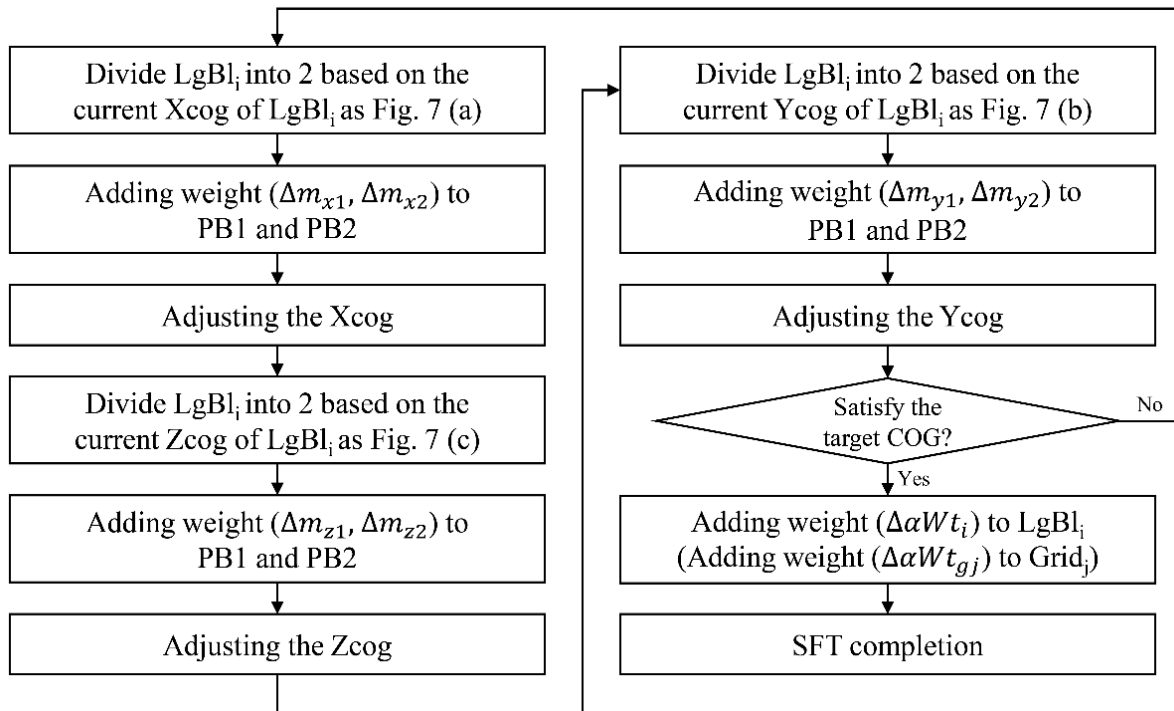


Figure 6. Detailed process of adding weight to $LgBl_i$ and adjusting the COG for the SFT.

In Equations (5)–(5.a), $\alpha Wt_{gix,k}$ is the weight added to $Grid_j$ for the SFT and adjustment of Xcog in the k^{th} iteration, and $\alpha Wt_{gij,k}$ and $\alpha Wt_{giz,k}$ are the weights added for the SFT and adjustment of Ycog and Zcog, respectively. Figure 8 shows the weight added to $Grid_j$ in the k^{th} iteration, prior to the addition of the weight; the grid weight is m_{gj} , whereas it is $m_{gj} + \alpha Wt_{gj,k}$ after weight addition.

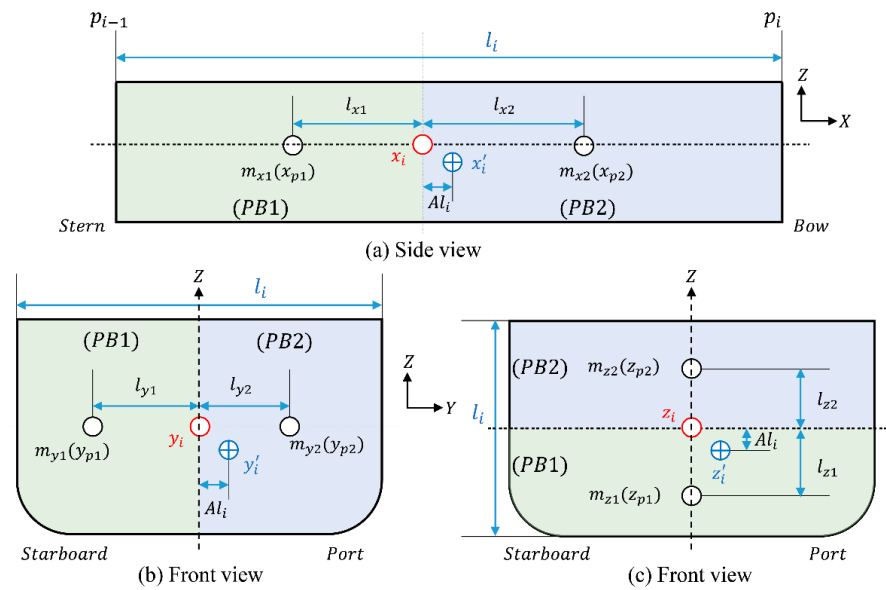


Figure 7. Dividing $LgBl_i$ into two partial blocks based on the current $LgBl_i$ COG location for the SFT. The $LgBl_i$ is divided according to the current (a) Xcog (longitudinal), (b) Ycog (transverse), and (c) Zcog (height) locations within the block.

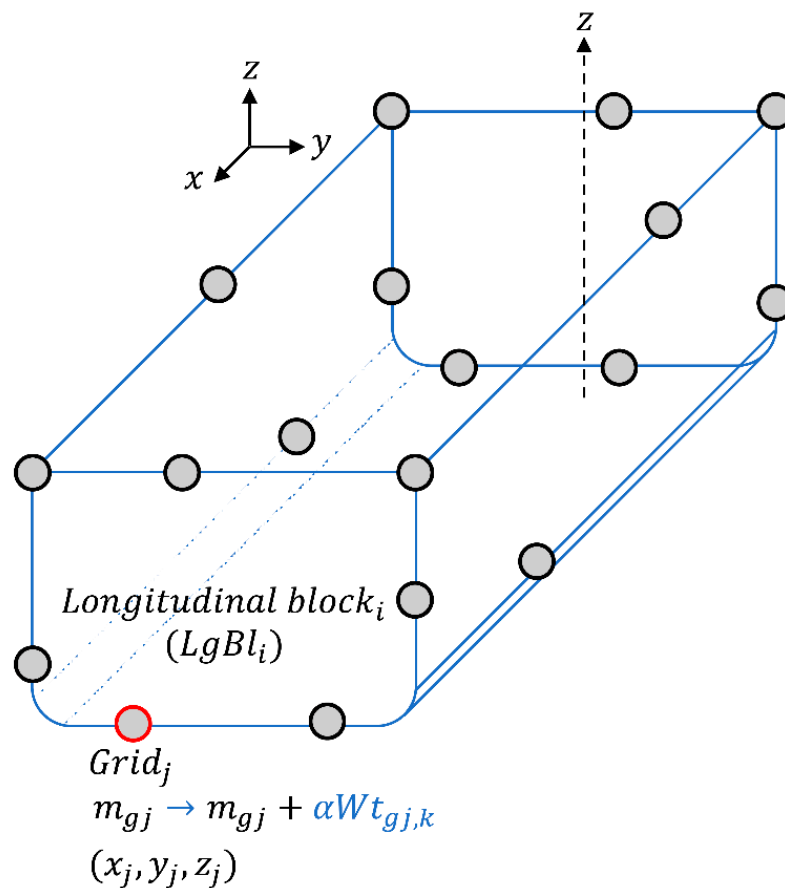


Figure 8. Change in the weight of the grid in $LgBl_i$ for SFT in the k^{th} iteration.

The weight added to $LgBl_i$ in the k^{th} iteration in Equations (5)–(5.a) and (6)–(6.a) is $\alpha W t_{i,k}$, which is equal to the sum of the weight added ($\alpha W t_{g_j,k}$) to $Grid_j$ in the k^{th} iteration. Further, the total weight added to the grid during the entire iteration is the same as the weight added ($\sum_{k=1}^m \alpha W t_{i,k}$) to $LgBl_i$ during the entire iteration. When completing the

iteration, the COG satisfies the target value; however, the SF does not satisfy the target value. Therefore, the weight ($\Delta\alpha Wt_i$) is added to $LgBl_i$ using Equations (6)–(6.b) such that the total weight added to the $LgBl_i$ becomes αWt_i , and consequently, the SF is tuned to the target value. At this moment, to keep the COG of the $LgBl$ to the target value, the weight ($\Delta\alpha Wt_i$) is distributed and assigned to the grid included in the $LgBl$ using Equations (6)–(6.b), and the added weight to the grid is $\Delta\alpha Wt_{gj}$.

$$\begin{aligned} \Delta\alpha Wt_i &= \alpha Wt_i - \sum_{k=1}^m \alpha Wt_{i,k} \quad (m = \text{Total iteration number by SFT at } LgBl_i) \\ &= \sum_{j=1}^n \Delta\alpha Wt_{gj} \quad (n = \text{Number of grids in } LgBl_i) \end{aligned} \tag{6}$$

$$\alpha Wt_{i,k} = \sum_{j=1}^n \alpha Wt_{gj,k} \quad (n = \text{Number of grids in } LgBl_i) \tag{6.a}$$

$$\Delta\alpha Wt_{gj} = \frac{\text{Current weight of Grid}_j}{\text{Current weight of } LgBl_i} \times \Delta\alpha Wt_i \tag{6.b}$$

where

$\Delta\alpha Wt_i = \alpha$ additional weight of $LgBl_i$ after completion of iteration for SFT

$\alpha Wt_i = (\text{Total}) \alpha$ additional weight of $LgBl_i$ for SFT

$\alpha Wt_{i,k} = k^{\text{th}}$ α additional weight of PB in $LgBl_i$ for SFT

$k = \text{Iteration number}$

$\Delta\alpha Wt_{gj} = \alpha$ additional weight of Grid_j after completion of iteration for SFT

If the SF and COG of all $LgBl$ s are adjusted in this way, the total weight, SF, and COG of the ship FE model can meet the target values. Upon completion of SFT, the SFT results and the BM value are examined through global ship analysis. If the total weight, COG, and SF curve of the ship FE model satisfy the target values, the BM value will also satisfy the target value. However, there exist cases where the BM cannot satisfy the target tolerance. In such cases, BMT is performed.

2.2.2. Detailed Process of the BMT

The detailed process of BMT for the ship FE model that has completed SFT is as follows. Because the ship FE model that has completed SFT satisfies the target values for the weight, COG, and SF, the COG of each $LgBl$ must be adjusted for BMT while maintaining the current status of these values. Thus, the BMT value at each DP of the ship FE model is calculated using the BM values obtained from the global ship model analysis, longitudinal BM curve of the ship obtained from the TnS data, and grid weight information. This is required to tune the current BM of the ship FE model to the TnS ship BM. To perform BMT using the calculated values, the movement distance required for the COG of each $LgBl$ is calculated. Figure 9 and Equations (7)–(7.g) show the method of calculating the BMT value and COG when the ship FE model is separated into three sections. The BM is calculated in the direction from the stern to the bow, as in SFT. In contrast to SFT, wherein αWt is added or subtracted, the COG is moved by adjusting the position and ratio of αWt distributed in each $LgBl$ without the addition of αWt for BMT. Moreover, regarding $LgBl_1$ and the DP of p_1 , when X_{cog} changes from x'_1 to x''_1 during BMT, the BM changes by ΔBM_1 and meets the target value of BM'_1 at BM_1 , while the weight of $LgBl_1$ is maintained at m'_1 . Here, as the

Ycog and Zcog of each LgBl were tuned to the target Ycog and Zcog values, the transverse (Ycog) and height (Zcog) components of the ship FE model COG location also coincided with the target values. Further, if the BM of $LgBl_2$ and p_2 and that of $LgBl_3$ and p_3 are tuned in the same method, the BM of the ship FE model coincides with the target TnS BM. Moreover, the weight and COG are maintained at the target values.

$$\begin{aligned} \Delta BM_1 &= BM'_1 - BM_1 \\ &= m'_1(p_1 - x''_1) - m'_1(p_1 - x'_1) \\ &= m'_1(x'_1 - x''_1) \end{aligned} \tag{7}$$

$$\begin{aligned} x''_1 &= \frac{m'_1 x'_1 - \Delta BM_1}{m'_1} \\ &= x'_1 - \frac{m'_1}{\Delta BM_1} \end{aligned} \tag{7.a}$$

$$\begin{aligned} \Delta BM_2 &= BM'_2 - BM_2 \\ &= m'_1(p_2 - x''_1) + m'_2(p_2 - x''_2) - \{m'_1(p_2 - x'_1) + m'_2(p_2 - x'_2)\} \\ &= m'_1(x'_1 - x''_1) + m'_2(x'_2 - x''_2) \end{aligned} \tag{7.b}$$

$$\begin{aligned} x''_2 &= \frac{m'_2 x'_2 - \Delta BM_2}{m'_2} + \frac{m'_1(x'_1 - x''_1)}{m'_2} \\ &= x'_2 - \frac{\Delta BM_2}{m'_2} + \frac{m'_1(x'_1 - x''_1)}{m'_2} \end{aligned} \tag{7.c}$$

$$\begin{aligned} \Delta BM_3 &= BM'_3 - BM_3 \\ &= m'_1(p_3 - x''_1) + m'_2(p_3 - x''_2) + m'_3(p_3 - x''_3) \\ &\quad - \{m'_1(p_3 - x'_1) + m'_2(p_3 - x'_2) + m'_3(p_3 - x'_3)\} \\ &= m'_1(x'_1 - x''_1) + m'_2(x'_2 - x''_2) + m'_3(x'_3 - x''_3) \end{aligned} \tag{7.d}$$

$$x''_3 = x'_3 - \frac{\Delta BM_3}{m'_3} + \frac{m'_1(x'_1 - x''_1) + m'_2(x'_2 - x''_2)}{m'_3} \tag{7.e}$$

$$x_M = \frac{m'_1 x'_1 + m'_2 x'_2 + m'_3 x'_3}{M'} = x_T \tag{7.f}$$

$$x_T = \frac{m'_1 x''_1 + m'_2 x''_2 + m'_3 x''_3}{M'} = x_M \tag{7.g}$$

where

m'_i = Weight of $LgBl_i$ model before BMT

M' = $m'_1 + m'_2 + m'_3$ (Weight of the global ship model)

x'_i = Xcog of $LgBl_i$ model before BMT

x''_i = Xcog of $LgBl_i$ model after BMT

BM_i = Model bending moment at p_i

BM'_i = TnS bending moment at p_i

ΔBM_i = BMT value at p_i

x_M = Xcog of the global ship model

$x_T = \text{Target Xcog of the global ship model}$

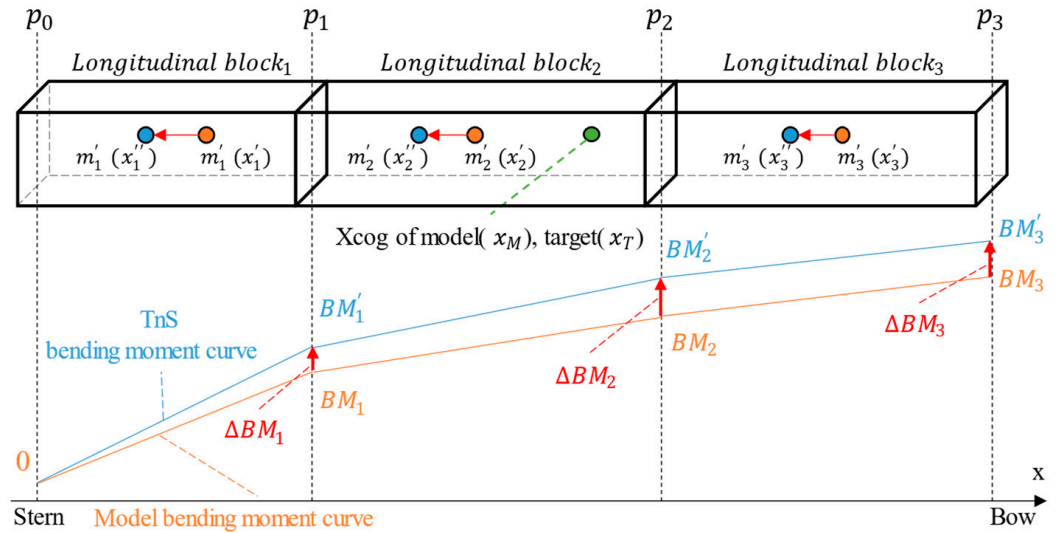


Figure 9. Calculation of the BMT value (ΔBM_i) using the TnS and model BM by global ship analysis. Calculation of the $LgBl_i$ target Xcog x'_i using ΔBM_i to correspond to the ship FE model Xcog (x_M) to the target Xcog (x_T) through the BMT.

The detailed method for adjusting the COG of each $LgBl$ for BMT is the same as that of the SFT method explained in Figure 6. Similar to 10% of Δm_{x1} or Δm_{x2} being added to $PB1$ or $PB2$ for SFT, 10% of the current $LgBl$ weight (m'_i) was added to $PB1$ or $PB2$ for BMT. The weight added to the grid included in each PB is calculated using Equations (8) and (8.a), and that added to $Grid_j$ in the h^{th} iteration is $\alpha Wt_{gj,h}$. This process is repeated until the COG (x'_i, y'_i, z'_i) of the $LgBl$ satisfies the target value (x''_i, y''_i, z''_i). Upon completion of the iterations, although the COG satisfies the target value, the BM cannot satisfy the target value.

$$\alpha Wt_{gix,h} = \frac{\text{Current weight of Grid}_j}{m'_i} \times 0.1m'_i \tag{8}$$

$$\alpha Wt_{gj,h} = \alpha Wt_{gix,h} + \alpha Wt_{gij,h} + \alpha Wt_{giz,h} \tag{8.a}$$

where

$$\alpha Wt_{gj,h} = h^{th} \alpha \text{ additional weight of Grid}_j \text{ for BMT}$$

$$\alpha Wt_{gix,h} = h^{th} \alpha \text{ additional weight of Grid}_j \text{ for BMT, Xcog}$$

$$\alpha Wt_{gij,h} = h^{th} \alpha \text{ additional weight of Grid}_j \text{ for BMT, Ycog}$$

$$\alpha Wt_{giz,h} = h^{th} \alpha \text{ additional weight of Grid}_j \text{ for BMT, Zcog}$$

$h = \text{Iteration number}$

$m'_i = \text{Current weight of LgBl}_i$

Therefore, the excess weight ($\Delta \gamma Wt_i$) is removed from the $LgBl$ such that the weight of the $LgBl$ is equal to the weight prior to BMT (weight after SFT). At this moment, excess

weight ($\Delta\gamma Wt_{gj}$) is removed from the grid in the LgBl using Equations (9)–(9.b) to maintain the COG of the LgBl at the target value.

$$\begin{aligned} \Delta\gamma Wt_i &= \sum_{h=1}^o \alpha Wt_{i,h} \quad (o = \text{Total iterations by BMT at LgBl}_i) \\ &= \sum_{j=1}^n \Delta\gamma Wt_{gj} \quad (n = \text{Number of grids in LgBl}_i) \end{aligned} \tag{9}$$

$$\alpha Wt_{i,h} = \sum_{j=1}^n \alpha Wt_{gj,h} \quad (n = \text{Number of grids in LgBl}_i) \tag{9.a}$$

$$\Delta\gamma Wt_{gj} = \frac{\text{Current weight of Grid}_j}{\text{Current weight of LgBl}_i} \times \Delta\gamma Wt_i \tag{9.b}$$

where

$\Delta\gamma Wt_i = \gamma$ removal weight of LgBl_i after completion of iteration for BMT

$\alpha Wt_{i,h} = h^{\text{th}}$ α additional weight of PB in LgBl_i by BMT

$h =$ Iteration number

$\Delta\gamma Wt_{gj} = \gamma$ removal weight of Grid_j after completion of iteration for BMT

Equations (10) and (10.a) represent the final αWt that is added to LgBl_i and Grid_j in LgBl_i following the application of SFT and BMT. If the SF, BM, and COG satisfy the target values by SFT, the weight $\sum_{h=1}^o \alpha Wt_{gj,h} - \Delta\gamma Wt_{gj}$ that is added to the grid based on the BMT in Equation (10.a) becomes zero.

$$\begin{aligned} \alpha Wt_i &= \sum_{k=1}^m \alpha Wt_{i,k} + \Delta\alpha Wt_i \quad \left(\sum_{h=1}^o \alpha Wt_{i,h} - \Delta\gamma Wt_i = 0 \right) \\ &= \sum_{j=1}^n \alpha Wt_{gj} \quad (n = \text{Number of grids in LgBl}_i) \end{aligned} \tag{10}$$

$$\begin{aligned} \alpha Wt_{gj} &= \sum_{k=1}^m \alpha Wt_{gj,k} + \Delta\alpha Wt_{gj} + \sum_{h=1}^o \alpha Wt_{gj,h} - \Delta\gamma Wt_{gj} \\ (m &= \text{Total iterations by SFT}) \\ (o &= \text{Total iterations by BMT}) \end{aligned} \tag{10.a}$$

where

$\alpha Wt_{ij} =$ (Total) α additional weight of LgBl_i by SFT and BMT

$\alpha Wt_{gj} =$ (Total) α additional weight of Grid_j by SFT and BMT

Thus, by adjusting the BM and COG of all LgBl_s, the total weight, COG, SF, and BM of the ship FE model can coincide with the required target values.

3. Results

3.1. Global Ship FE Model for Tuning the SF and BM

The accuracy of the SF, BM, weight, and COG were examined before and after performing SFT and BMT for the ship FE model using the developed algorithm. An oil shuttle tanker model, shown in Figure 10, was used to test and verify the accuracy of the SFT and BMT algorithms. The full-size FE model geometry and main dimensions of the shuttle tanker are in Table 1 (Lim et al., 2022) [6]. The ship FE model had an overall length (L_{OA}),

breadth (B), and depth of 277.8, 49, and 24.5 m, respectively, divided into 168,120 grids with 357,673 elements.

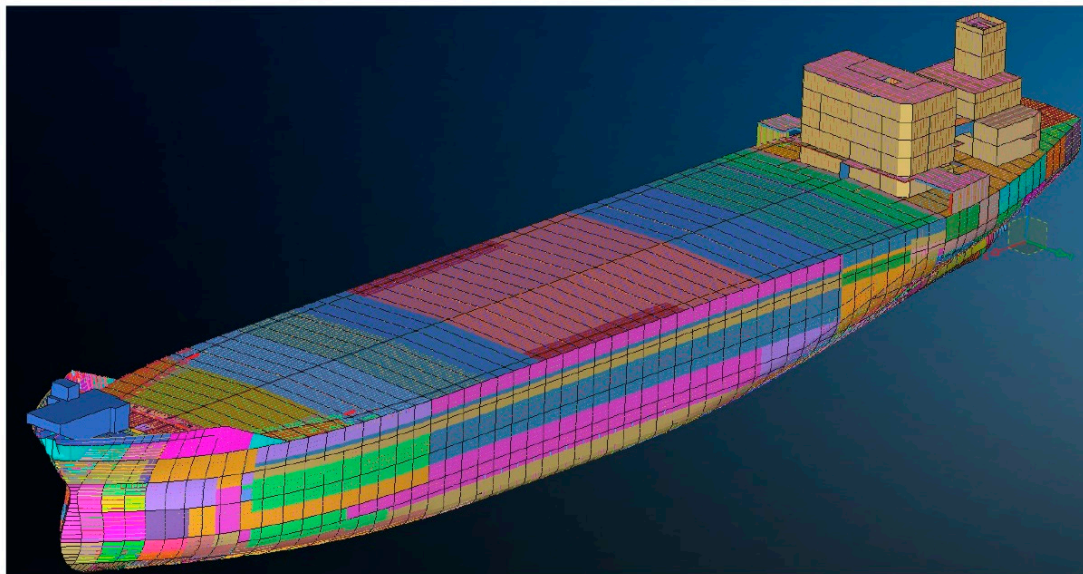


Figure 10. Global ship FE model of oil shuttle tanker used for algorithm validation.

Table 1. Main dimensions and information of ship FE model.

Ship Type	LOA	Breadth	Depth
Oil shuttle tanker	277.8 m	49 m	24.5 m

Table 2 lists the target weight and COG component values for the ship FE model along with the weight and COG before SFT (after the WD). The weight of the ship FE model relative to the target weight is expressed using the unit PU, calculated using Equation (11). The distances between each coordinate (Xcog, Ycog, and Zcog) of the target COG and the COG of the ship FE model before SFT were 0.2707, 0.0171, and 0.0766 m, respectively, with a model weight of 1.0063 PU of the target weight. Thus, the condition of the ship FE model before SFT sufficiently satisfied the target values for the global ship analysis.

Table 2. Weight and COG components for the target and ship FE model before SFT.

Value	Weight (PU)	Xcog (m)	Ycog (m)	Zcog (m)
Target	1.0000	119.9770	−0.1880	14.4790
Before SFT	1.0063	120.2477	−0.1709	14.4024

Table 3 presents the model weight and COG results before and after the application of SFT and BMT. Figures 11–16 show the SF and BM results for the ship FE model before and after the application of SFT and BMT. The associated graph data and errors are also presented in Tables 4–9. In each graph, the x-axis represents the longitudinal direction position of the ship; the x-coordinate of zero corresponds to the after perpendicular of the stern. The SF and BM values are expressed in PU using the weight notation method of the ship FE model. In addition, of all the TnS values, which are the target values for each tuning case, the largest absolute value was used as the reference value. The errors in each table were calculated using the differences between the model and TnS values. The PU for the SF and BM and the error were calculated using Equations (11)–(11.b).

$$Weight (PU) = \frac{Weight_{Model}}{Weight_{Target}} \tag{11}$$

$$\text{Shear force, Bending moment (PU)} = \frac{\text{Model value}_i - \text{TnS value}_i}{\text{TnS value}_{ABS \max}} \tag{11.a}$$

$$\text{Error} = \left| \frac{\text{Model value}_i - \text{TnS value}_i}{\text{TnS value}_i} \right| \times 100 \tag{11.b}$$

where

$\text{Weight}_{\text{Model}} = \text{Weight of global ship model}$

$\text{Weight}_{\text{Target}} = \text{Target weight}$

$\text{Model value}_i = \text{Model shear force or bending moment at } i\text{th division position}$

$\text{TnS value}_i = \text{TnS shear force or bending moment at } i\text{th division position}$

$\text{TnS value}_{ABS \max} = \text{Maximum absolute value of TnS shear force or bending moment}$

Table 3. Weight, COG target value, and results of SFT and BMT.

Status	Ballast Condition				Full Load Condition			
	Weight (PU)	Xcog (m)	Ycog (m)	Zcog (m)	Weight (PU)	Xcog (m)	Ycog (m)	Zcog (m)
Target value	1.0000	119.9770	−0.1880	14.4790	1.0000	119.9770	−0.1880	14.4790
Before SFT	1.0063	120.2477	−0.1709	14.4024	1.0063	120.2477	−0.1709	14.4024
After SFT	1.0063	120.2477	−0.1710	14.4023	1.0063	120.2475	−0.1707	14.4028
After BMT	1.0063	120.2477	−0.1723	14.4190	1.0063	120.2475	−0.1708	14.4030

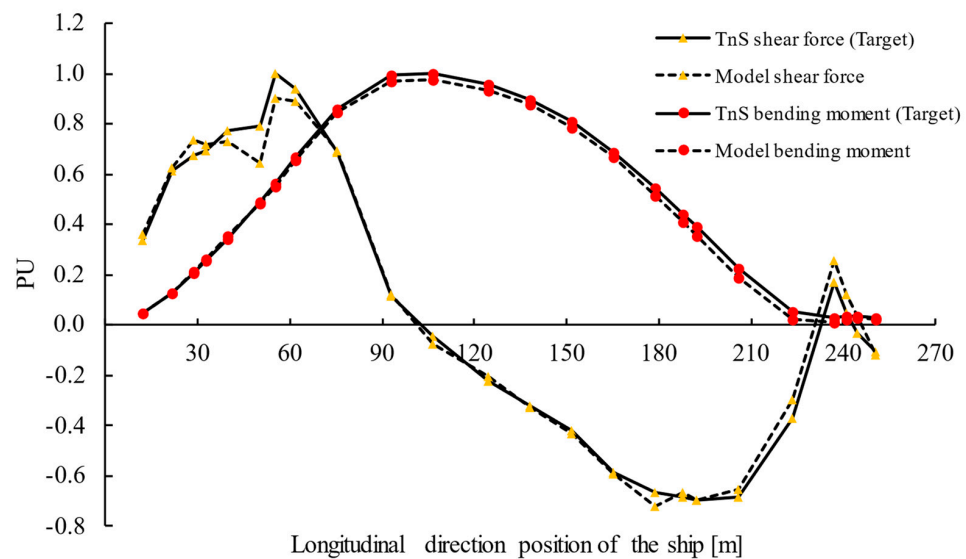


Figure 11. SF and BM curves of the TnS data and ship FE model at each DP before SFT under the ballast condition.

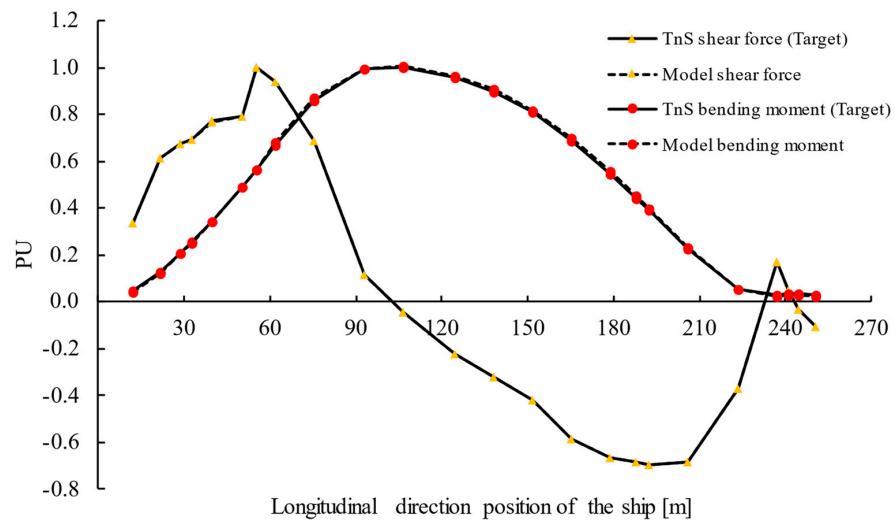


Figure 12. SF and BM curves of the TnS data and ship FE model at each DP after SFT (before BMT) under the ballast condition.

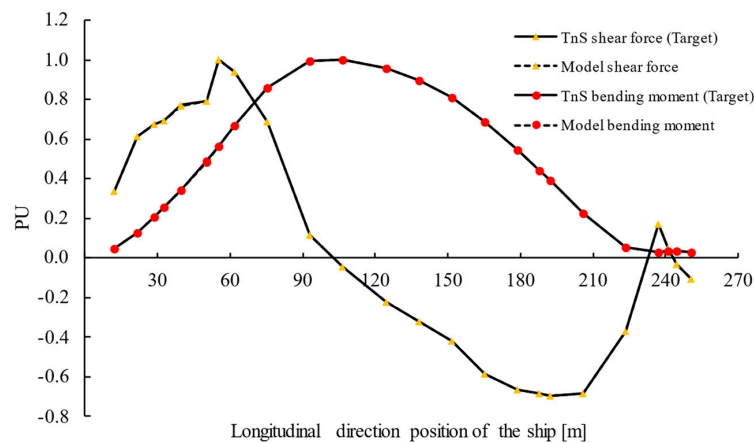


Figure 13. SF and BM curves of the TnS data and ship FE model at each DP after BMT under the ballast condition.

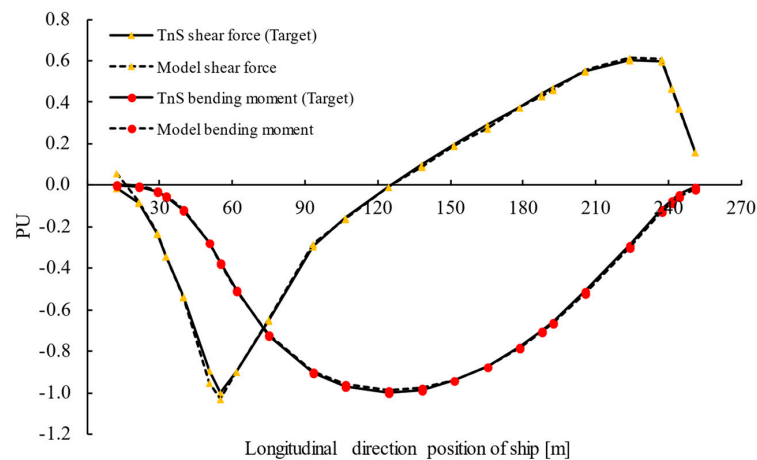


Figure 14. SF and BM curves of the TnS data and ship FE model at each DP before SFT under the full load condition.

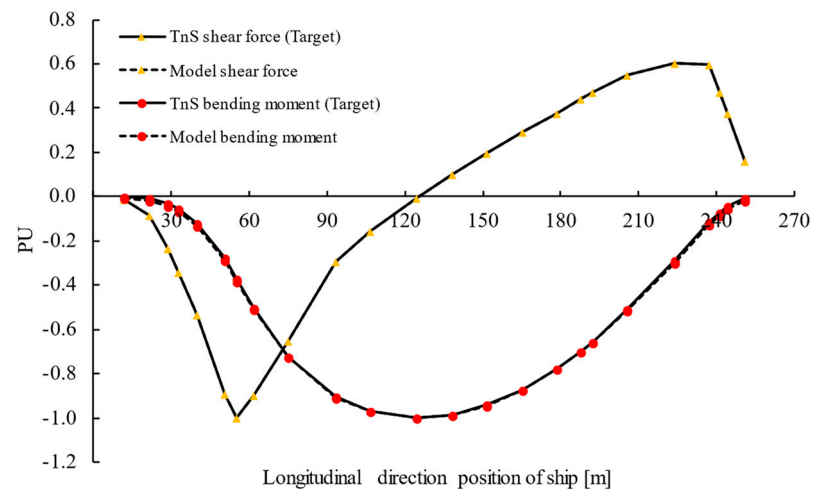


Figure 15. SF and BM curves of the TnS data and ship FE model at each DP after SFT (before BMT) under the full load condition.

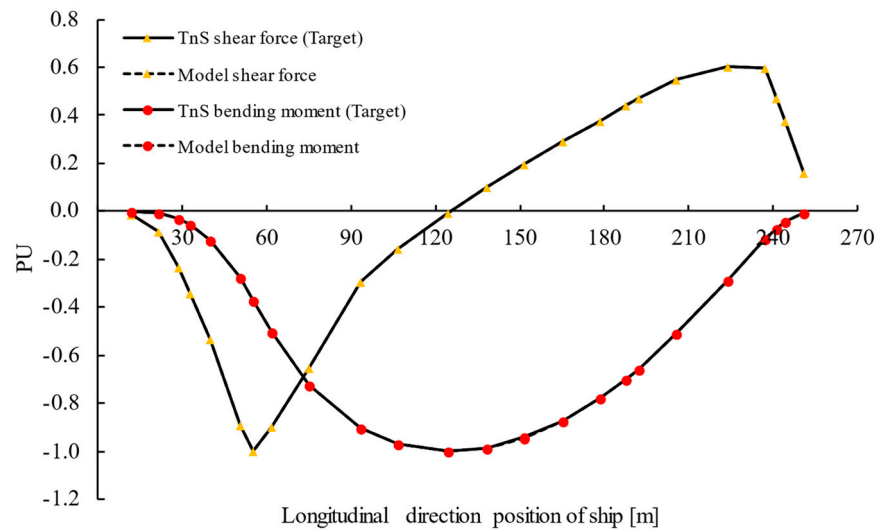


Figure 16. SF and BM curves of the TnS data and ship FE model at each DP after BMT under the full load condition.

Table 4. SF, BM, and error of the TnS data and ship FE model before SFT under the ballast condition.

DP (m)	SF			BM		
	TnS (PU)	Model (PU)	Error (%)	TnS (PU)	Model (PU)	Error (%)
12	0.3385	0.3641	7.5500	0.0449	0.0463	3.2606
21.6	0.6123	0.6283	2.6156	0.1264	0.1281	1.3824
28.8	0.6739	0.7348	9.0418	0.2070	0.2157	4.2228
32.8	0.6937	0.7155	3.1438	0.2541	0.2649	4.2613
40	0.7730	0.7311	5.4138	0.3438	0.3539	2.9276
50.4	0.7915	0.6438	18.6606	0.4873	0.4852	0.4350
55.2	1.0000	0.9011	9.8899	0.5613	0.5529	1.4917

Table 4. *Cont.*

DP (m)	SF			BM		
	TnS (PU)	Model (PU)	Error (%)	TnS (PU)	Model (PU)	Error (%)
61.7	0.9368	0.8874	5.2787	0.6696	0.6574	1.8324
75.2	0.6874	0.6914	0.5933	0.8613	0.8453	1.8641
93.2	0.1160	0.1203	3.6578	0.9914	0.9692	2.2401
106.7	−0.0455	−0.0732	60.9939	1.0000	0.9788	2.1188
124.7	−0.2225	−0.2066	7.1364	0.9587	0.9330	2.6803
138.2	−0.3200	−0.3242	1.2960	0.8961	0.8786	1.9554
151.7	−0.4197	−0.4345	3.5415	0.8111	0.7831	3.4499
165.2	−0.5851	−0.5916	1.1095	0.6901	0.6661	3.4754
178.7	−0.6654	−0.7217	8.4626	0.5457	0.5135	5.9153
187.7	−0.6818	−0.6676	2.0897	0.4425	0.4074	7.9450
192.2	−0.6964	−0.6972	0.1185	0.3898	0.3548	8.9901
205.7	−0.6863	−0.6538	4.7360	0.2280	0.1881	17.4778
223.7	−0.3692	−0.2943	20.2785	0.0526	0.0237	54.9932
237.2	0.1702	0.2540	49.2646	0.0270	0.0119	55.7607
241.2	0.0497	0.1205	142.4491	0.0346	0.0250	27.8002
244.4	−0.0328	0.0378	215.3379	0.0352	0.0288	18.2176
250.8	−0.1057	−0.1189	12.4643	0.0276	0.0250	9.5497

Table 5. SF, BM, and error of the TnS data and ship FE model after SFT (before BMT) under the ballast condition.

DP (m)	SF			BM		
	TnS (PU)	Model (PU)	Error (%)	TnS (PU)	Model (PU)	Error (%)
12	0.3385	0.3389	0.1182	0.0449	0.0435	3.0940
21.6	0.6123	0.6123	0.0017	0.1264	0.1219	3.5271
28.8	0.6739	0.6739	0.0017	0.2070	0.2045	1.2152
32.8	0.6937	0.6937	0.0017	0.2541	0.2507	1.3419
40	0.7730	0.7660	0.9023	0.3438	0.3404	0.9862
50.4	0.7915	0.7915	0.0012	0.4873	0.4896	0.4791
55.2	1.0000	1.0000	0.0007	0.5613	0.5666	0.9377
61.7	0.9368	0.9368	0.0009	0.6696	0.6782	1.2845
75.2	0.6874	0.6874	0.0007	0.8613	0.8715	1.1839
93.2	0.1160	0.1160	0.0032	0.9914	0.9947	0.3340
106.7	−0.0455	−0.0455	0.0044	1.0000	1.0071	0.7140
124.7	−0.2225	−0.2225	0.0002	0.9587	0.9645	0.6016
138.2	−0.3200	−0.3200	0.0008	0.8961	0.9091	1.4430
151.7	−0.4197	−0.4197	0.0005	0.8111	0.8157	0.5658
165.2	−0.5851	−0.5851	0.0005	0.6901	0.7014	1.6489
178.7	−0.6654	−0.6654	0.0005	0.5457	0.5555	1.7876

Table 5. *Cont.*

DP (m)	SF			BM		
	TnS (PU)	Model (PU)	Error (%)	TnS (PU)	Model (PU)	Error (%)
187.7	−0.6818	−0.6818	0.0005	0.4425	0.4534	2.4551
192.2	−0.6964	−0.6964	0.0004	0.3898	0.4002	2.6488
205.7	−0.6863	−0.6863	0.0006	0.2280	0.2313	1.4447
223.7	−0.3692	−0.3692	0.0009	0.0526	0.0517	1.6756
237.2	0.1702	0.1702	0.0006	0.0270	0.0222	17.9298
241.2	0.0497	0.0497	0.0016	0.0346	0.0298	13.8203
244.4	−0.0328	−0.0328	0.0015	0.0352	0.0298	15.3904
250.8	−0.1057	−0.1057	0.0005	0.0276	0.0229	16.9229

Table 6. SF, BM, and error of the TnS data and ship FE model after BMT under the ballast condition.

DP (m)	SF			BM		
	TnS (PU)	Model (PU)	Error (%)	TnS (PU)	Model (PU)	Error (%)
12	0.3385	0.3391	0.1691	0.0449	0.0448	0.1534
21.6	0.6123	0.6123	0.0040	0.1264	0.1262	0.0982
28.8	0.6739	0.6739	0.0035	0.2070	0.2069	0.0660
32.8	0.6937	0.6937	0.0038	0.2541	0.2539	0.0537
40	0.7730	0.7659	0.9165	0.3438	0.3437	0.0412
50.4	0.7915	0.7915	0.0042	0.4873	0.4872	0.0280
55.2	1.0000	1.0000	0.0036	0.5613	0.5612	0.0251
61.7	0.9368	0.9369	0.0040	0.6696	0.6695	0.0198
75.2	0.6874	0.6874	0.0064	0.8613	0.8612	0.0158
93.2	0.1160	0.1161	0.0426	0.9914	0.9913	0.0102
106.7	−0.0455	−0.0454	0.1159	1.0000	0.9999	0.0086
124.7	−0.2225	−0.2225	0.0246	0.9587	0.9586	0.0073
138.2	−0.3200	−0.3200	0.0176	0.8961	0.8961	0.0067
151.7	−0.4197	−0.4196	0.0127	0.8111	0.8110	0.0068
165.2	−0.5851	−0.5850	0.0083	0.6901	0.6900	0.0058
178.7	−0.6654	−0.6654	0.0070	0.5457	0.5457	0.0056
187.7	−0.6818	−0.6818	0.0060	0.4425	0.4425	0.0064
192.2	−0.6964	−0.6963	0.0058	0.3898	0.3898	0.0057
205.7	−0.6863	−0.6863	0.0049	0.2280	0.2280	0.0071
223.7	−0.3692	−0.3692	0.0060	0.0526	0.0526	0.0163
237.2	0.1702	0.1702	0.0070	0.0270	0.0270	0.0120
241.2	0.0497	0.0497	0.0184	0.0346	0.0346	0.0070
244.4	−0.0328	−0.0328	0.0221	0.0352	0.0352	0.0057
250.8	−0.1057	−0.1057	0.0038	0.0276	0.0276	0.0062
12	−0.0127	0.0583	559.8927	0.0005	0.0031	587.5897
21.6	−0.0828	−0.0800	3.3737	−0.0067	0.0013	120.1511

Table 7. SF, BM, and error of the TnS data and ship FE model before SFT under the full load condition.

DP (m)	SF			BM		
	TnS (PU)	Model (PU)	Error (%)	TnS (PU)	Model (PU)	Error (%)
28.8	−0.2356	−0.2258	4.1622	−0.0301	−0.0223	25.8677
32.8	−0.3400	−0.3418	0.5557	−0.0544	−0.0472	13.1915
40	−0.5331	−0.5417	1.6211	−0.1212	−0.1153	4.8087
50.4	−0.8946	−0.9513	6.3369	−0.2758	−0.2770	0.4554
55.2	−1.0000	−1.0324	3.2370	−0.3720	−0.3759	1.0509
61.7	−0.8962	−0.8990	0.3171	−0.5027	−0.5067	0.7942
75.2	−0.6528	−0.6460	1.0284	−0.7249	−0.7199	0.6880
93.2	−0.2957	−0.2818	4.7007	−0.9063	−0.8983	0.8822
106.7	−0.1561	−0.1614	3.3437	−0.9701	−0.9582	1.2260
124.7	−0.0048	−0.0081	70.6826	−1.0000	−0.9898	1.0193
138.2	0.1024	0.0870	15.0214	−0.9861	−0.9788	0.7398
151.7	0.1981	0.1887	4.7091	−0.9431	−0.9410	0.2232
165.2	0.2888	0.2753	4.6792	−0.8732	−0.8751	0.2241
178.7	0.3730	0.3738	0.2053	−0.7786	−0.7840	0.6950
187.7	0.4402	0.4272	2.9478	−0.7010	−0.7073	0.8961
192.2	0.4714	0.4590	2.6262	−0.6575	−0.6661	1.2939
205.7	0.5460	0.5547	1.6107	−0.5117	−0.5234	2.2689
223.7	0.6046	0.6152	1.7516	−0.2881	−0.3006	4.3185
237.2	0.5963	0.6075	1.8625	−0.1168	−0.1282	9.7491
241.2	0.4684	0.4663	0.4456	−0.0718	−0.0831	15.7269
244.4	0.3749	0.3703	1.2333	−0.0432	−0.0554	28.0790
250.8	0.1598	0.1583	0.9361	−0.0078	−0.0199	156.3072

Table 8. SF, BM, and error of the TnS data and ship FE model after SFT (before BMT) under the full load condition.

DP (m)	SF			BM		
	TnS (PU)	Model (PU)	Error (%)	TnS (PU)	Model (PU)	Error (%)
12	−0.0127	−0.0120	5.1498	0.0005	−0.0072	1687.3114
21.6	−0.0828	−0.0828	0.0245	−0.0067	−0.0163	142.9273
28.8	−0.2356	−0.2355	0.0138	−0.0301	−0.0408	35.8468
32.8	−0.3400	−0.3399	0.0115	−0.0544	−0.0662	21.7294
40	−0.5331	−0.5335	0.0806	−0.1212	−0.1335	10.2235
50.4	−0.8946	−0.8945	0.0077	−0.2758	−0.2879	4.3821
55.2	−1.0000	−0.9999	0.0077	−0.3720	−0.3828	2.9009
61.7	−0.8962	−0.8961	0.0095	−0.5027	−0.5118	1.8116
75.2	−0.6528	−0.6527	0.0152	−0.7249	−0.7259	0.1307
93.2	−0.2957	−0.2956	0.0407	−0.9063	−0.9078	0.1639
106.7	−0.1561	−0.1560	0.0825	−0.9701	−0.9690	0.1044

Table 8. *Cont.*

DP (m)	SF			BM		
	TnS (PU)	Model (PU)	Error (%)	TnS (PU)	Model (PU)	Error (%)
124.7	−0.0048	−0.0046	2.8505	−1.0000	−0.9988	0.1156
138.2	0.1024	0.1025	0.1311	−0.9861	−0.9853	0.0826
151.7	0.1981	0.1982	0.0665	−0.9431	−0.9437	0.0642
165.2	0.2888	0.2889	0.0427	−0.8732	−0.8745	0.1586
178.7	0.3730	0.3731	0.0303	−0.7786	−0.7812	0.3344
187.7	0.4402	0.4403	0.0235	−0.7010	−0.7034	0.3406
192.2	0.4714	0.4715	0.0207	−0.6575	−0.6609	0.5140
205.7	0.5460	0.5460	0.0146	−0.5117	−0.5171	1.0545
223.7	0.6046	0.6046	0.0084	−0.2881	−0.2979	3.3859
237.2	0.5963	0.5964	0.0050	−0.1168	−0.1285	10.0436
241.2	0.4684	0.4684	0.0049	−0.0718	−0.0839	16.9518
244.4	0.3749	0.3749	0.0048	−0.0432	−0.0561	29.7041
250.8	0.1598	0.1598	0.0062	−0.0078	−0.0202	159.8586

Table 9. SF, BM, and error of the TnS data and ship FE model after BMT under the full load condition.

DP (m)	SF			BM		
	TnS (PU)	Model (PU)	Error (%)	TnS (PU)	Model (PU)	Error (%)
12	−0.0127	−0.0113	10.5398	0.0005	0.0013	188.5672
21.6	−0.0828	−0.0828	0.0058	−0.0067	−0.0062	6.7113
28.8	−0.2356	−0.2356	0.0022	−0.0301	−0.0297	1.2199
32.8	−0.3400	−0.3400	0.0015	−0.0544	−0.0540	0.6274
40	−0.5331	−0.5319	0.2211	−0.1212	−0.1209	0.2312
50.4	−0.8946	−0.8946	0.0006	−0.2758	−0.2756	0.0794
55.2	−1.0000	−1.0000	0.0006	−0.3720	−0.3718	0.0487
61.7	−0.8962	−0.8962	0.0006	−0.5027	−0.5026	0.0308
75.2	−0.6528	−0.6528	0.0009	−0.7249	−0.7249	0.0072
93.2	−0.2957	−0.2957	0.0019	−0.9063	−0.9062	0.0022
106.7	−0.1561	−0.1561	0.0031	−0.9701	−0.9701	0.0030
124.7	−0.0048	−0.0048	0.1033	−1.0000	−1.0001	0.0090
138.2	0.1024	0.1024	0.0044	−0.9861	−0.9862	0.0134
151.7	0.1981	0.1981	0.0020	−0.9431	−0.9433	0.0181
165.2	0.2888	0.2888	0.0013	−0.8732	−0.8734	0.0236
178.7	0.3730	0.3730	0.0009	−0.7786	−0.7788	0.0310
187.7	0.4402	0.4402	0.0005	−0.7010	−0.7013	0.0371
192.2	0.4714	0.4714	0.0006	−0.6575	−0.6578	0.0407
205.7	0.5460	0.5460	0.0004	−0.5117	−0.5120	0.0552
223.7	0.6046	0.6046	0.0001	−0.2881	−0.2884	0.0930
237.2	0.5963	0.5963	0.0001	−0.1168	−0.1170	0.1839

Table 9. *Cont.*

DP (m)	SF			BM		
	TnS (PU)	Model (PU)	Error (%)	TnS (PU)	Model (PU)	Error (%)
241.2	0.4684	0.4684	0.0001	−0.0718	−0.0720	0.2694
244.4	0.3749	0.3749	0.0001	−0.0432	−0.0434	0.4017
250.8	0.1598	0.1598	0.0001	−0.0078	−0.0079	1.6419

3.2. Results of SFT and BMT under the Ballast Condition

The results of the analysis of the ship FE model under the ballast condition, before and after the application of SFT, are shown in Figures 11 and 12, respectively, while the results after the BMT are shown in Figure 13. As shown in Figure 11, the SF and BM curves of the ship FE model subjected only to the WD exhibit similar trends as those of the TnS data; however, the target values were not satisfied in certain areas before SFT. In particular, the SF curve of the accommodation area located on the stern side within the range of 12–75 m was significantly different from that of the TnS data. Moreover, the SF curve on the bow side at positions > 170 m exhibited a significant difference from that of the TnS data. Table 4 shows that the SF error was the largest (215.3379%) at 244.4 m. Here, the SF was approximately 3.3% of the maximum absolute value of the TnS SF. Further, the BM curve on the bow side at positions > 90 m was less consistent with the TnS data compared to that on the stern side at positions ≤ 90 m. In particular, Table 4 shows that the BM error was the largest (55.7607%) at 237.2 m. In this instance, the BM was approximately 1.2% of the maximum absolute value of the TnS BM. Thus, the SF and BM curves were found to have different error occurrence locations.

As shown in Figure 12, the SF and BM curves of the ship FE model were more consistent with those of the TnS data after SFT than before SFT. In particular, the SF exhibited very high accuracy. The dotted line expressing the SF curve of the ship FE model is highly consistent with the solid line curve of the TnS data, resulting in the two curves appearing as one curve along the entire length. Table 5 shows that the SF error was the largest (0.9023%) at 40 m. Here, the model SF was relatively high, approximately 76.60% of the maximum absolute value of the TnS SF. In addition, the error did not exceed 0.0044% along the entire length, except for the 0.9023 and 0.1182% errors at the 40 and 12 m positions, respectively. The accuracy of the BM increased following the SFT application. In particular, the error between the BM curve of the ship FE model and that of the TnS data decreased on the bow side at positions > 90 m, and the number of sections where the dotted line overlapped the solid line increased. As shown in Table 5, the maximum error of the BM in the midship part of the hull did not exceed 2.7%, except for the stern side positions < 21.6 m and those on the bow side at >237.2 m. Further, the bow side positions > 237.2 m exhibited larger errors than those on the stern side at <21.6 m, and the maximum error (17.9298%) was observed at 237.2 m. Thus, the accuracy of the SF was found to increase significantly following the application of SFT, while the accuracy of the BM also improved.

As shown in Figure 13, the SF and BM curves of the ship FE model were highly consistent with those of the TnS data following the BMT application. The respective SF and BM curves appear as one curve each, along their entire lengths, indicating that the BMT was successful and that the high accuracy of the SF curve was maintained. Table 6 shows that the largest SF error (0.9165%) occurred at 40 m, which is the same position that exhibited a high error in the results associated with performing only SFT, as given in Table 5. Further, for the ship FE model, the maximum SF and BM errors did not exceed 0.9165 and 0.1534%, respectively. Moreover, the average SF and BM errors were 0.0591 and 0.0258%, respectively, indicating that very high accuracy was obtained using the algorithm to perform SFT and BMT for the ship FE model under a ballast condition. In addition, Table 3 shows that not only the weight of the ship FE model under the ballast condition but also the COG remained constant before and after SFT and after BMT.

3.3. Results of SFT and BMT under the Full Load Condition

The analysis results of the full load condition of the ship FE model before and after the application of SFT are shown in Figures 14 and 15, respectively, while the results after BMT are shown in Figure 16. As shown in Figure 14, the SF and BM curves of the ship FE model before SFT were analogous to those of the TnS data. Similar to the ballast condition, the BM curve was more consistent than the SF curve, which exhibited low accuracy on the stern side at positions <60 m. Table 7 shows that the SF and BM errors exceeded 500% at 12 m. This is because the model SF was 5.83% of the maximum absolute value of the TnS SF, with a sign opposite to that of the TnS SF. In addition, the BM error was relatively large because both the ship FE model and TnS data had very small BM values. Thus, when the SF and BM values are very small compared to the maximum absolute values of the TnS data, substantial errors may occur despite the small differences.

As shown in Figure 15, the SF and BM curves of the ship FE model were more consistent with those of the TnS data after SFT than before SFT. In particular, the SF curve was more consistent than the BM curve. The results of the BM curve were more consistent under the full load condition than the ballast condition. Consequently, the respective SF and BM curves for the ship FE model and TnS data each appear as one curve along the entire length. Comparing the BM curves of the ship FE model and TnS data, slight differences were observed on the stern side at positions < 60 m. Table 8 shows that the SF error decreased from 559.8927% before SFT to 5.1498% after SFT at the 12 m position; however, the BM error increased approximately 2.8 times from 587.5897 to 1687.3114% at this position. Moreover, because the TnS BM is extremely small (0.05% of the maximum absolute value of the TnS BM) at 12 m, a large error occurred despite fine tuning. In addition, the BM error was large (159.8586%) at the 250.8 m position on the bow side. The TnS BM at this position was also very small, 0.78% of the maximum absolute value of the TnS BM. Thus, the SFT results under the full load condition were found to be more accurate than or similar to the SFT results under the ballast condition, except for the values associated with the positions at both ends, the bow and stern.

Figure 16 shows the BMT results. The SF and BM curves of the ship FE model were highly consistent with those of the TnS data. Further, the results in Figure 16 were more consistent than those in Figure 15, and even the small errors observed on the bow and stern sides were not visible, rendering the respective SF and BM curves as one curve each, along their entire lengths. This indicates that the BMT was successful and that the high accuracy of the SF curve was maintained. Table 9 shows that the BM error decreased by approximately 8.9 times from 1687.3114 to 188.5672% at the 12 m position associated with the largest error. In contrast, at the same position, the SF error increased from 5.1498 to 10.5398%. Both the SF and BM exhibited maximum errors at the 12 m location. Further, all the errors on the bow side at locations > 237.2 m decreased, and the maximum values did not exceed 1.6419%. In addition, the maximum errors of the 32.8–241.2 m positions, excluding those positions where the SF and BM values were relatively small, did not exceed 0.66274%. The average SF and BM errors were 0.4538 and 8.3478%, respectively. Thus, except for the 12 m position where the SF and BM values were very small, the accuracy obtained using the algorithm to perform SFT and BMT for the ship FE model under the full load condition can be concluded to be very high. Table 3 shows that not only the weight of the ship FE model under the full load condition but also the COG remained constant before and after SFT and after BMT.

3.4. Limitations of the Research

The errors in the tuning results of the SF and BM under ballast and full load conditions are mainly due to the method of distributing the weight of elements divided at the LgBl DP to the grids.

Two methods of distributing and calculating the weight of structural beam elements to the grid can be used. One is the method used in this study, and the other is an improved method. The method of distributing the weight used in the study is shown in Figure 17

and Equations (12)–(12.c). The vertical dotted lines represent the DPs. The weight of the structural beam element (M_{beam}) across the LgBl DPs is equally allocated to *Grid1* and *Grid2*, and αWt is calculated and distributed to both grids using Equations (12)–(12.c). Figure 18 and Equations (13)–(13.g) describe the improved method. After dividing and calculating the beam weight considering the DPs, the beam weight is distributed to A1 and A2, which are the COGs of both divided beams. Subsequently, αWt is calculated and distributed to both grids. In the first method (Figure 17), because the WD and COG tuning of the structural member considering the DPs are inaccurate, the αWt distribution is also inaccurate, causing errors in the SF and BM. Therefore, errors also occur in the ship FE model. In the improved method (Figure 18), if the beam weight can be distributed to A1 and A2, and αWt is calculated and distributed considering the DPs, the ship FE model weight, COG, SF, and BM errors will be reduced, and more accurate tuning is possible.

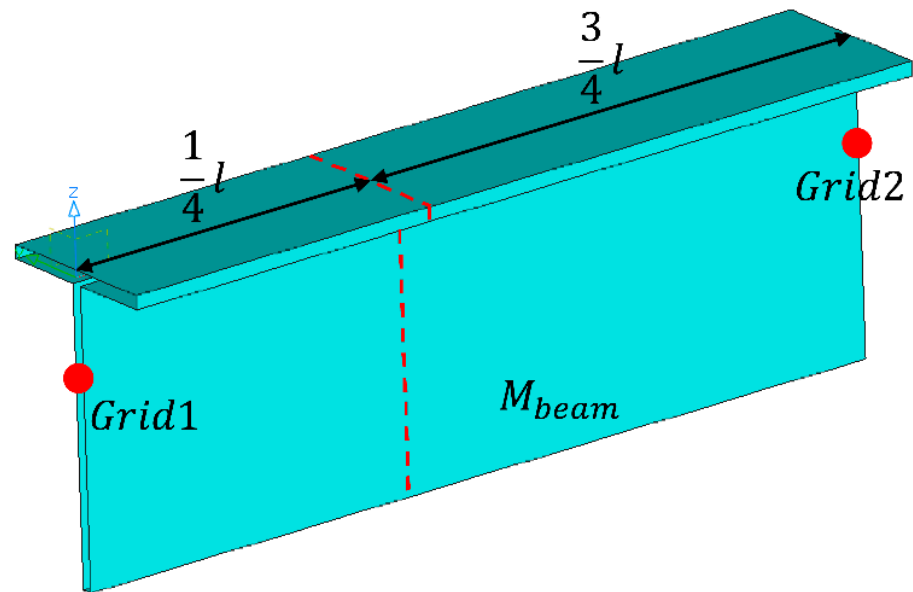


Figure 17. A beam weight distribution method using Equation (12) in this study.

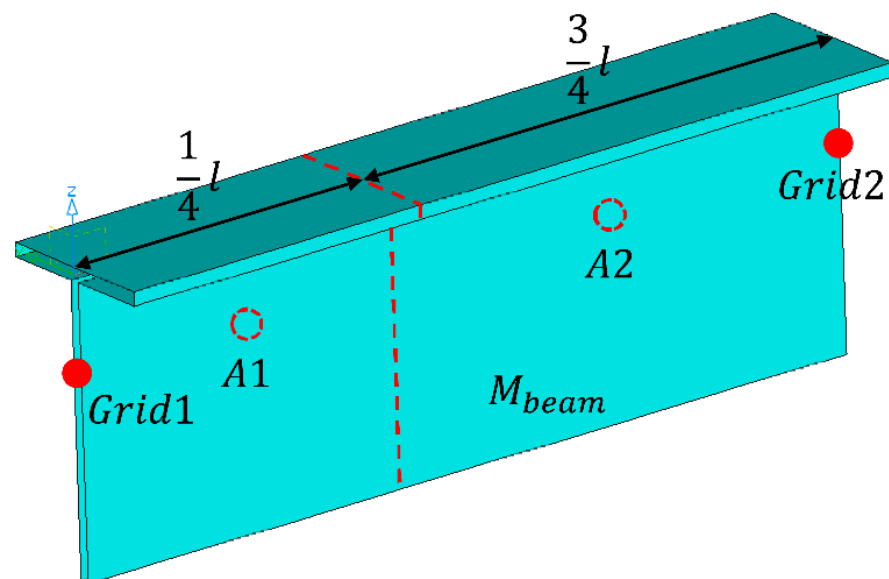


Figure 18. An improved beam weight distribution method using Equation (13).

As indicated in Table 6, which presents the SFT and BMT results for the ship FE model under a ballast condition, the SF and BM at each DP satisfied a tolerance of less than 5%.

However, Table 9, which presents the ship FE model results under a full load condition, shows that the SF and BM errors did not satisfy the tolerance at the 12 m position. In particular, the BM showed a considerable error of 188.5672%. In Figure 16, illustrating the results in Table 9, the BM curves of the ship FE model and TnS appear to coincide at 12 m. However, at this position, the BM values of the ship FE model and TnS were very small. The model BM was 0.13% of the maximum absolute value of the TnS BM, while the TnS BM was 0.05% of the maximum absolute value. Consequently, these very small values caused relatively large errors despite a small change. In addition, the BM at 10 m showed an error of 6.7113%, which was higher than the tolerance, and exhibited the same characteristics as described above.

For the assessment of structural safety using the ship FE model, areas with relatively small SF and BM values, such as the 12 m position, are not areas of interest. The main areas of interest are those with large absolute values of SF and BM. Therefore, even if the SF and BM values exceed the error tolerance, if the values themselves are small, they are not considered rigorously in the structural safety assessment and, thus, are regarded as exceptions. The SFT and BMT results under ballast and full load conditions show that the values at positions where the error exceeded 5% were mostly very small compared to the maximum absolute value. Further, the tuning results exhibited larger errors under a full load condition than under a ballast condition, while the stern showed larger errors than the bow under each condition.

$$Grid1\ weight_{(Before\ tuning)} = \frac{M_{beam}}{2} + AddWt_{g1} \tag{12}$$

$$Grid2\ weight_{(Before\ tuning)} = \frac{M_{beam}}{2} + AddWt_{g2} \tag{12.a}$$

$$Grid1\ weight_{(After\ tuning)} = \frac{M_{beam}}{2} + AddWt_{g1} + \alpha Wt_{g1} \tag{12.b}$$

$$Grid2\ weight_{(After\ tuning)} = \frac{M_{beam}}{2} + AddWt_{g2} + \alpha Wt_{g2} \tag{12.c}$$

$$A1\ weight_{(Before\ tuning)} = \frac{1}{4} M_{beam} \tag{13}$$

$$A2\ weight_{(Before\ tuning)} = \frac{3}{4} M_{beam} \tag{13.a}$$

$$Grid1\ weight_{(Before\ tuning)} = AddWt_{g1} \tag{13.b}$$

$$Grid2\ weight_{(Before\ tuning)} = AddWt_{g2} \tag{13.c}$$

$$A1\ weight_{(After\ tuning)} = \frac{1}{4} M_{beam} \tag{13.d}$$

$$A2\ weight_{(After\ tuning)} = \frac{3}{4} M_{beam} \tag{13.e}$$

$$Grid1\ weight_{(After\ tuning)} = AddWt_{g1} + \alpha Wt_{g1} \tag{13.f}$$

$$Grid2\ weight_{(After\ tuning)} = AddWt_{g2} + \alpha Wt_{g2} \tag{13.g}$$

where

$$M_{beam} = T - Beam\ weight$$

$AddWt_{gj}$ = Additional weight of Grid_j by weight distribution

αWt_{gj} = α additional weight of Grid_j by SFT or BMT

4. Conclusions

The ship FE model used in global ship analysis must satisfy the longitudinal SF and BM under the loading conditions of the ship. For this, SFT and BMT must be performed for the ship FE model using the TnS data of the ship to allow the model to exhibit SF and BM curves that coincide with those of the ship. In addition, the ship FE model weight and COG must be tuned to the required target values. Thus, in this study, we proposed and developed a C#-based algorithm of SFT and BMT. The accuracy of the new algorithm was analyzed and compared using the ship FE model of an oil shuttle tanker, and the accuracy under a ballast condition was compared with that under a full load condition. The longitudinal positions where an SF and BM check are required for the ship FE model were designated. Based on each position, the model was divided into LgBl, and SFT and BMT were performed. The results are as follows:

- (1) Before SFT, the SF and BM curves of the ship FE model under a ballast condition exhibited tendencies similar to those of TnS; however, the SF and BM curves significantly deviated from the TnS values (target values) in the accommodation area on the stern side and the area on the bow side, respectively. However, following SFT, the SF and BM curves of the ship FE model more closely coincided with those of TnS. Although the BM curve exhibited slight differences, the SF curve of the ship FE model was highly consistent with that of the TnS. Further, the curves of the model and TnS appeared as one curve because they were highly consistent with each other. Following BMT, the SF and BM curves of the ship FE model became more consistent with the TnS curves, indicating that the BMT was successful and that it maintained the high accuracy of the SF curve.

Regarding the SF and BM curves of the ship FE model under a full load condition before SFT, the latter was more consistent than the former in a manner similar to the ballast condition. Following SFT, the SF and BM curves of the ship FE model were more consistent with those of TnS. Although slight differences were observed on the stern side similar to in the ballast condition, the curves of the model overlapped those of TnS, thus appearing as one curve. Following BMT, the SF and BM curves of the ship FE model were highly consistent with the TnS curves in the entire area, except for the errors at the 12 m position.

- (2) Under a ballast condition, the ship FE model exhibited a maximum SF error of 215.3379% at 244.4 m and a maximum BM error of 55.7607% at 237.2 m before SFT. After SFT, the SF error at 244.4 m significantly decreased from 215.3379% to 0.0015%, and the maximum error was 0.1182% at 12 m. The BM error at 237.2 m significantly decreased from 55.7607% to 17.9298%, which was the maximum error. After BMT, the SF error at 12 m slightly increased from 0.1182% to 0.1691%, which was the maximum error. The BM error at 237.2 m significantly decreased from 17.9298% to 0.0120%, and a maximum error of 0.1534% occurred at 12 m, which exhibited the maximum SF error.

Under a full load condition, the ship FE model exhibited a maximum SF error of 559.8927% at 12 m and a maximum BM error of 587.5897% at the same position before SFT. After SFT, the SF error at 12 m significantly decreased from 559.8927% to 5.1498%, which was the maximum error. The BM error at the same position significantly increased from 587.5897% to 1687.3114%, which was the maximum error. After BMT, the SF error at 12 m increased from 5.1498% to 10.5398%, which was the maximum error. The BM error at the same position decreased from 1687.3114% to 188.5672%, which was the maximum error. Under a ballast condition and a full load condition, not only the weight of the ship FE

model but also the COG remained constant at the target values before and after SFT and after BMT.

Under a ballast condition, the ship FE model exhibited very small errors and high accuracy at all positions following the application of SFT and BMT. In contrast, under a full load condition, the SF and BM of the model exceeded the tolerance at 12 m. However, the SF and BM at the position exhibited large errors despite a relatively small change because they were very small compared to the maximum absolute values. Such areas with small values are regarded as exceptions even if the values exceed the tolerance because they are outside the area of interest and thus are not considered carefully in the assessment of structural safety using global ship analysis.

In the above results, the errors of the SF and BM occurred due to WD errors that did not consider the LgBl DPs. Accuracy can be further improved if the WD, SF, and BM are adjusted in consideration of the LgBl DPs. The proposed algorithm is a generalized algorithm for a shuttle tanker (liquid cargo ship). A program including automatic functions was developed to easily use the proposed algorithm. The time required for SFT and BMT using the proposed algorithm takes from a few minutes to an hour, whereas not using the algorithm takes a few days. In addition, the advantage of using the algorithm is that it can achieve high accuracy. Further, the SFT and BMT results under ballast and full load conditions satisfy the weight, SF, BM, and COG conditions required for global ship analysis; therefore, the developed SFT and BMT algorithms are expected to be utilized in global ship analysis. In the future, an SFT and BMT algorithm for the global ship analysis of container ships and offshore plants other than oil carriers must be developed. Therefore, research on an SFT and BMT algorithm for container ships will be conducted.

Author Contributions: C.L.: conceptualization, data curation, investigation, methodology, software; I.-s.H.: data curation, funding acquisition, validation; J.-Y.K.: data curation, validation; I.-j.B. and B.L.: data curation, validation; J.S.P.: validation, writing—review and editing; S.-c.S.: conceptualization, funding acquisition, investigation, project administration, supervision. All authors have read and agreed to the published version of the manuscript.

Funding: This work was supported by the Korea Institute of Energy Technology Evaluation and Planning (KETEP), the Ministry of Trade, Industry, and Energy (MOTIE) of the Republic of Korea (no. 20224000000090), and the Korea Evaluation Institute Of Industrial Technology (KEIT) and the Ministry of Trade, Industry, and Energy (MOTIE) of the Republic of Korea (no. 20018667, Development of Integrated Ship Design System for Hull, Compartment, Basic Calculation, and Loading Guidance Based on Artificial Intelligent Technology). The funders had no role in the study design, data collection and analysis, decision to publish, or preparation of the manuscript.

Institutional Review Board Statement: Not applicable.

Informed Consent Statement: Not applicable.

Data Availability Statement: Not applicable.

Conflicts of Interest: The authors declare no conflict of interest.

References

1. Biondi, B.; Muscolino, G.; Sidoti, A. Methods for Calculating Bending Moment and Shear Force in the Moving Mass Problem. *J. Vib. Acoust.* **2004**, *126*, 542–552. [[CrossRef](#)]
2. Cho, H.; Choi, S.; Joo, K. A Study on the Global Vibration Analysis Method of the Commercial Vessels. *Trans. Korean Soc. Noise Vib. Eng.* **2008**, *18*, 509–515. [[CrossRef](#)]
3. Kim, D.-m. Effects of Operational Condition and Sea States on Wave-Induced Bending Moments of Large Merchant Vessels. *J. Soc. Nav. Arch. Korea* **2003**, *40*, 60–67. [[CrossRef](#)]
4. Kim, I.I.; Choi, J.H.; Jo, H.J.; Suh, H.W. A development of data structure and mesh generation algorithm for global ship analysis modeling system. *Korean J. Comp. Des. Eng.* **2005**, *10*, 61–69. [[CrossRef](#)]
5. Du Kim, J.; Jang, B.-S.; Yun, R.-H.; Jeong, H.-S. Improvement of the bending behavior of a flexible riser: Part I I-Hysteretic Modeling of Bending Stiffness in Global Dynamic Analysis. *Appl. Ocean Res.* **2020**, *101*, 102249. [[CrossRef](#)]
6. Kim, S.; Ryue, J.; Park, I.-K. Prediction of the wave induced second order vertical bending moment due to the variation of the ship side angle by using the quadratic strip theory. *Int. J. Nav. Arch. Ocean Eng.* **2018**, *10*, 259–269. [[CrossRef](#)]

7. Kim, Y.S.; Kim, J.H.; Kim, B.W. A study on Wave Loads acting on a Containership in Waves (II). In Proceedings of the Korean Institute of Navigation and Port Research Autumn Conference, Incheon, Republic of Korea, 16–17 December 2008; Volume 32, pp. 284–285.
8. Kövesdi, B.; Jáger, B.; Dunai, L. Bending and shear interaction behavior of girders with trapezoidally corrugated webs. *J. Constr. Steel Res.* **2016**, *121*, 383–397. [[CrossRef](#)]
9. Kwon, Y.S. On the characteristics of still-water and wave bending moments with the variations of ship weight distribution. *J. Ocean Eng. Technol.* **1996**, *10*, 3–13.
10. Lee, S.C.; Doh, D.H.; Goo, J.S. Analysis of wave loads of ships with advancing speed in regular waves. *J. Korea Soc. Power Syst. Eng.* **2010**, *14*, 53–58.
11. Lim, C.; Han, I.-S.; Park, B.-C.; Oh, S.-J.; Kim, G.-Y.; Shin, S.-C. Weight distribution algorithm for global ship analysis in preliminary design stage. *J. Comput. Des. Eng.* **2022**, *9*, 907–918. [[CrossRef](#)]
12. Liu, B.; Soares, C.G. Ultimate strength assessment of ship hull structures subjected to cyclic bending moments. *Ocean Eng.* **2020**, *215*, 107685. [[CrossRef](#)]
13. Mansour, A.; D'Oliveira, J.M. Hull Bending Moment Due to Ship Bottom Slamming in Regular Waves. *J. Ship Res.* **1975**, *19*, 80–92. [[CrossRef](#)]
14. Moreira, L.; Soares, C.G. Neural network model for estimation of hull bending moment and shear force of ships in waves. *Ocean Eng.* **2020**, *206*, 107347. [[CrossRef](#)]
15. MSC Software Corporation. MSC NASTRAN 2018 Quick Reference Guide. 2018. Available online: www.mssoftware.com (accessed on 22 September 2023).
16. Park, H.-S.; Choi, S.-H.; Lee, Y.-S. A Study on Vibration Analysis Method Using the Global Structural Analysis Model. *J. Soc. Nav. Arch. Korea* **2007**, *44*, 314–322. [[CrossRef](#)]
17. Pesterev, A.V.; Tan, C.A.; Bergman, L.A. A New Method for Calculating Bending Moment and Shear Force in Moving Load Problems. *J. Appl. Mech.* **2001**, *68*, 252–259. [[CrossRef](#)]
18. Rahman, M.K.; Chowdhury, M. Estimation of Ultimate Longitudinal Bending Moment of Ships and Box Girders. *J. Ship Res.* **1996**, *40*, 244–257. [[CrossRef](#)]
19. Recupero, A.; D'aveni, A.; Ghersi, A. Bending Moment–Shear Force Interaction Domains for Prestressed Concrete Beams. *J. Struct. Eng.* **2005**, *131*, 1413–1421. [[CrossRef](#)]
20. Valtonen, V.; Bond, J.; Hindley, R. Improved method for non-linear FE analysis of polar class ship primary structures. *Mar. Struct.* **2020**, *74*, 102825. [[CrossRef](#)]
21. Wang, C.; Wu, J.; Wang, D. Design similar scale model of a 10,000 TEU container ship through combined ultimate longitudinal bending and torsion analysis. *Appl. Ocean Res.* **2019**, *88*, 1–14. [[CrossRef](#)]
22. Waskito, K.T.; Kashiwagi, M.; Iwashita, H.; Hinatsu, M. Prediction of nonlinear vertical bending moment using measured pressure distribution on ship hull. *Appl. Ocean Res.* **2020**, *101*, 102261. [[CrossRef](#)]
23. Xu, J.; Haddara, M. Estimation of wave-induced ship hull bending moment from ship motion measurements. *Mar. Struct.* **2001**, *14*, 593–610. [[CrossRef](#)]
24. Xu, S.; Liu, B.; Garbatov, Y.; Wu, W.; Soares, C.G. Experimental and numerical analysis of ultimate strength of inland catamaran subjected to vertical bending moment. *Ocean Eng.* **2019**, *188*, 106320. [[CrossRef](#)]
25. Yun, R.H.; Jang, B.S.; Du Kim, J.D. Improvement of the bending behavior of a flexible riser: Part I—Nonlinear bending behavior considering the shear deformation of polymer layers. *Appl. Ocean Res.* **2020**, *101*, 102249. [[CrossRef](#)]

Disclaimer/Publisher's Note: The statements, opinions and data contained in all publications are solely those of the individual author(s) and contributor(s) and not of MDPI and/or the editor(s). MDPI and/or the editor(s) disclaim responsibility for any injury to people or property resulting from any ideas, methods, instructions or products referred to in the content.